AUG 1983
RECEIVED
NASA STI FACILITY
ACCESS DEPT.

AXIAL VANE-TYPE SWIRLER PERFORMANCE

CHARACTERISTICS

(NASA-CR-172995) AXIAL VANE-TYPE SWIRLER PERFORMANCE CHARACTERISTICS M.S. Thesis (Oklahoma State Univ., Stillwater.) 120 p HC A06/MF A01 CSCL 21E

N83-32808

Unclas
G3/07 15013

By

GLENN FERRIS SANDER

Bachelor of Science in Mechanical Engineering

Oklahoma State University

Stillwater, Oklahoma

1982

Submitted to the Faculty of the Graduate College
of the Oklahoma State University
in partial fulfillment of the requirements
for the Degree of
MASTER OF SCIENCE
July, 1983

NAG 3-74

AXIAL VANE-TYPE SWIRLER PERFORMANCE CHARACTERISTICS

By

GLENN FERRIS SANDER

Bachelor of Science in Mechanical Engineering

Oklahoma State University

Stillwater, Oklahoma

1982

Submitted to the Faculty of the Graduate College
of the Oklahoma State University
in partial fulfillment of the requirements
for the Degree of
MASTER OF SCIENCE
July, 1983

Name: Glenn F. Sander Date of Degree: July, 1983

Institution: Oklahoma State University Location: Stillwater, Oklahoma

Title of Study: AXIAL VANE-TYPE SWIRLER PERFORMANCE CHARACTERISTICS

Pages in Study: 107 Candidate for Degree of Master of Science

Major Field: Mechanical Engineering

Scope and Method of Study: The performance of an axial vane-type swirler was investigated to aid in computer modeling of gas turbine combustor flowfields and in evaluation of turbulence models for swirling confined jet flow. The swirler studied is annular with a hub-to-swirler diameter ratio of 0.25 and ten adjustable vanes of pitch-to-chord ratio 0.68. Measurements of time-mean axial, radial, and tangential velocities were made at the swirler exit plane using a five-hole pitot probe technique with computer data reduction. Nondimensionalized velocities from both radial and azimuthal traverses are tabulated and plotted for a range of swirl vane angles ϕ from 0 to 70 degrees. In addition, a study was done of idealized exit-plane velocity profiles relating the swirl numbers S and S' to the ratio of maximum swirl and axial velocities for each idealized case, and comparing the idealized swirl numbers with ones calculated from measured profiles.

Findings and Conclusions: Measurements of time-mean velocity components at the swirler exit plane show clearly the effects of centrifugal forces, recirculation zones, and blade wakes on the exit-plane velocity profiles. Assumptions of flat axial and swirl profiles are found to be progressively less realistic as the swirl vane angle increases, with axial and swirl velocities peaking strongly at the outer edges of the swirler exit and significant non-zero radial velocities present. Higher-order idealized profiles gave improved correspondence with moderate to high swirl cases, but none of the idealizations studied could approximate the measured profiles satisfactorily. For strong swirl, the central recirculation zone extended upstream of the exit plane, and nonaxisymmetry was found in all swirl cases investigated.

ADVISER'S APPROVAL David G. Lilley

AXIAL VANE-TYPE SWIRLER PERFORMANCE
CHARACTERISTICS

Thesis Approved:

David G. Lilley

Thesis Adviser

A. J. Ghajar

P. M. Moretti

Dean of the Graduate College

ACKNOWLEDGMENTS

The author would like to express his sincere gratitude to his major adviser, Dr. David G. Lilley, for his guidance and encouragement. Appreciation is also extended to the other members of the committee, Dr. Afshin J. Ghajar and Dr. Peter M. Moretti.

Thanks are due to Ms. Rhonda Thomson and Ms. Neisa Lock for typing the draft copy of the thesis, and to Ms. Rhonda Smith for typing the final copy.

The author also wishes to gratefully acknowledge financial support for the project from NASA Lewis Research Center and Air Force Wright Aeronautical Laboratories under NASA Grant No. NAG 3-74.

This study is dedicated to the author's parents, Dr. and Mrs. David A. Sander, for their loving concern and encouragement.

TABLE OF CONTENTS

Chapter	Page

LIST OF TABLES

ORIGINAL PAGE IS
OF POOR QUALITY

LIST OF FIGURES

NOMENCLATURE

English Symbols

c	blade chord width
d	swirler exit diameter
D	test section diameter
F	velocity ratio w_o/u_o for case I
G	axial flux of momentum; velocity ratio w_{mo}/u_o for case II
H,I,J	w_{mo}/u_{mo} for cases III - V
p	time-mean pressure, N/m^2 = Pa
s	blade spacing or pitch
S	swirl number = $G_\theta/(G_x d/2)$
u,v,w	axial, radial and tangential components of velocity
x,r,θ	axial, radial, azimuthal cylindrical polar coordinates
z	hub-to-swirler diameter ratio d_h/d

Greek Symbols

β	yaw angle of probe = $\tan^{-1}(w/u)$
δ	pitch angle of probe = $\tan^{-1}[v/(u^2 + w^2)^{1/2}]$
θ	azimuth angle
ρ	density
σ	pitch - to - chord ratio
ϕ	swirl vane angle = $\tan^{-1}(w_{in}/u_{in})$, assuming perfect vanes

Subscripts

atm	ambient atmospheric conditions
C,N,S,E,W	center, north, south, east, west pitot pressure ports
h	hub
in	inlet conditions, upstream of swirler
m	maximum profile value
o	value at swirler outlet
x	axial direction
θ	tangential direction
∞	reference value at edge of swirler exit

Superscripts

'	alternate form, neglecting pressure variation; fluctuating quantity
—	time-mean quantity

CHAPTER I

INTRODUCTION

1.1 Combustor Flowfield Investigations

The problem of optimizing gas turbine combustion chamber design is complex, because of the many conflicting design requirements. The need for a more complete understanding of the fluid dynamics of the flow in such combustion chambers has been recognized by designers in recent years, and research is continuing on several fronts to alleviate the problem.

As part of an on-going project at Oklahoma State University, studies are in progress concerned with experimental and theoretical research in 2-D axisymmetric geometries under low speed, nonreacting, turbulent, swirling flow conditions. The flow enters the test section and proceeds into a larger chamber (expansion ratio $D/d = 2$) via a sudden or gradual expansion (side-wall angle $\alpha = 90$ and 45 degrees). Inlet swirl vanes are adjustable to a variety of vane angles with $\phi = 0$, 38, 45, 60 and 70 degrees being emphasized. The general aim of the entire study is to characterize the time-mean and turbulence flowfield, recommend appropriate turbulence model advances, and implement and exhibit results of flowfield predictions. The present contribution concentrates on the time-mean flow characteristics being generated by the upstream annular swirler, using a five-hole pitot probe technique.

1.2 Previous Studies

Research is progressing in several areas related to the flow facility investigation just described. Computer simulation techniques are being used to study the effect of geometry and other parameter changes on the flowfield. An advanced computer code (1) has been developed to predict confined swirling flows corresponding to those studied experimentally. Tentative predictions (2) have now been supplemented by predictions made from realistic inlet conditions (3) for a complete range of swirl strengths with downstream nozzle effects (4). Accuracy of predictions from a computer model is strongly dependent on the inlet boundary conditions used, which are primarily determined by the swirler and its performance at different vane angle settings. In the earlier predictions, the velocity boundary conditions at the inlet to the model combustor were approximated by idealized flat profiles for axial and swirl velocity, with radial velocity assumed to be zero. However, recent measurements taken closer to the swirler exit show that the profiles produced are quite nonuniform, with nonzero radial velocity and nonaxisymmetry.

The flowfield in the test section is being characterized experimentally in a variety of ways. Flow visualization has been achieved via still (5) and movie (6) photography of neutrally buoyant helium-filled soap bubbles and smoke produced by an injector and a smoke wire. Time-mean velocities have been measured with a five-hole pitot probe at low (5) and high (7) swirl strengths. To help in turbulence modeling, complete turbulence measurements have been made on weakly (8) and strongly (9) swirling flows, using a six-orientation single-wire hot-wire technique. An alternative three-wire technique has also been shown to be useful in the complex flow situations (10).

References to previous work done elsewhere are found in Chapter II, relating to theoretical analysis of swirler performance.

1.3 Scope and Objectives

A key element in swirling flow studies is the swirl generator used. Since it lies at the inlet to the combustor model, the swirler can have a strong influence on the measurements or predictions made downstream. Better definition of the swirler's performance characteristics is needed.

In the present study, the main objective has been to make time-mean velocity measurements as close as possible to the swirler exit, so as to define more accurately the performance characteristics of the swirler. A range of swirl-blade angles ϕ from 0 to 70 deg. is considered. Specific objectives include:

1. Investigate the flow turning effectiveness of flat blades in annular axial vane swirlers at various blade angles, ϕ.
2. Investigate the degree of nonaxisymmetry introduced by vane-type swirlers.
3. Establish correlations between the blade angle ϕ and the velocity profiles and degree of swirl actually produced.
4. Evaluate the applicability of idealized velocity profiles used recently in flowfield prediction codes, and specify more realistic idealized profiles for future use.
5. Provide swirler exit data usable as inlet conditions in prediction codes being used to establish, evaluate, and improve turbulence models.

1.4 Outline of the Thesis

In the previous sections, the scope and objectives of this study were presented, with the significance of the study in relation to past and present work on combustor flowfield investigations being highlighted.

Chapter II describes mathematical derivations from idealized swirler exit velocity profiles, relating the swirl number to the ratio of maximum swirl and axial velocities for several cases.

Chapter III covers the experimental equipment and procedures used for measurement of the swirler exit flowfield. It includes descriptions of the flowfield facility, the swirler, and the five-hole pitot probe and its associated instrumentation. Calibration, measurement, and data reduction procedures are also briefly described.

The first two sections of Chapter IV discuss experimental results from radial and azimuthal traverses, respectively, noting the presence of nonaxisymmetry, recirculation, and strong velocity gradients at the swirler exit plane. A third section describes the results of a check on sensitivity of the measurements to calibration errors. The last section of Chapter IV compares the swirl numbers calculated from measured profiles and from the idealizations of Chapter II to judge the usefulness of the idealized profiles.

Chapter V presents conclusions drawn from the above results and makes recommendations for further research on this topic.

Appendixes A and B include tables and figures, respectively. A description of revisions to be computer program for reduction of five-hole pitot probe data is in Appendix C, and a listing of the program with sample input is in Appendix D.

CHAPTER II

IDEALIZED PROFILE DERIVATIONS

2.1 Idealized Velocity Profiles

All theoretical analyses of swirler performance and most numerical simulations of combustor flowfields have used simple idealized swirler exit velocity profiles. Common assumptions made include flat axial and swirl velocity profiles downstream of the swirler for swirlers with vanes of constant angle (2, 5, 11, 12), and flat axial profile with linear swirl profile (solid-body rotation) for swirlers with helicoidal vanes and for tangential-entry swirl generators (13, 14). These, however, have been shown to be quite unrealistic (3, 12, 15) and to lead to considerable errors in computer simulations (4). Although the best approach for numerical simulations is to use experimentally measured profiles if they are available, idealized profiles are very useful in theoretical work. If more realistic profile assumptions can be developed which are still mathematically tractable, more useful analytical results may be derived. Better idealized profiles would also be useful as inlet boundary conditions for computer modeling when measured data is not available.

Measurements have shown (3) that linear and parabolic profiles of axial velocity are more appropriate for moderate and high swirl cases, and that the swirl velocity also approaches a parabolic profile at high swirl strengths, with most of the flow leaving near the outer boundary of the swirler. Several combinations of linear and parabolic idealized profiles are shown in Figure 1, along with the flat and linear profile assumptions used in previous studies. Parameters associated with these profiles are investigated in Section 2.3.

2.2 Definition of Swirl Parameters

The swirl number is a nondimensional parameter used to characterize the degree of swirl generated by a swirler. It is defined as follows (13):

$$S = \frac{G_\theta}{G_x(d/2)} \tag{1}$$

where the axial flux of angular momentum G_θ is given by

$$G_\theta = \int_0^{2\pi} d\theta \int_0^{d/2} [\rho uw + \overline{\rho u'w'}]\, r^2\, dr \tag{2}$$

and the axial flux of axial momentum G_x is given by

$$G_x = \int_0^{2\pi} d\theta \int_0^{d/2} [\rho u^2 + \overline{\rho u'^2} + (p - p_\infty)]r\, dr \tag{3}$$

and d/2 is the swirler exit radius (4). These equations are obtained from appropriate manipulation of the axial and azimuthal momentum equations, respectively. In free jet flows these two expressions are invariant with respect to downstream location. In the axial momentum expression, the pressure term $(p - p_\infty)$ is given from radial integration of the radial momentum equation (16) by

$$(p - p_\infty) = \int_{d/2}^{r} [\rho w^2 \tfrac{1}{r}]\, dr - \overline{\rho v'^2} \tag{4}$$

If the pressure term is omitted from the axial momentum, the dynamic axial momentum flux G_x' is obtained:

$$G_x' = \int_0^{2\pi} d\theta \int_0^{d/2} [\rho u^2 + \overline{\rho u'^2}]\, r\, dr \tag{5}$$

This leads to an alternate definition of swirl number (17):

$$S' = \frac{G_\theta}{G'_x(d/2)} \tag{6}$$

If turbulent stress terms are neglected, it is apparent that a knowledge of the distribution of the time-mean u and w velocity components across the swirler is sufficient to calculate either swirl number. The idealized exit velocity profiles provide just such knowledge, and expressions relating swirl number to the ratio of maximum exit swirl and axial velocities can now be derived for each of the profile types. As the procedure is similar for each of the five cases, a detailed derivation will be shown for the first case only, with only final results given for the other four.

2.3 Swirl Numbers for Idealized Profiles

By assuming axisymmetric flow and neglecting turbulent stresses as stated previously, the definitions in Equations (2) through (4) reduce to

$$G_\theta = 2\pi \int_0^{d/2} [\rho uw] r^2 \, dr \tag{7}$$

$$G_x = 2\pi \int_0^{d/2} [\rho u^2 + (p - p_\infty)] r \, dr \tag{8}$$

and

$$(p - p_\infty) = \int_{d/2}^{r} [\rho w^2 \frac{1}{r}] dr \tag{9}$$

When the expressions for axial and swirl velocity for case I (see Figure 1) are substituted into Equation (7), one obtains

$$G_0 = \frac{2}{3}\pi\rho u_o w_o \,(d/2)^3 \tag{10}$$

Substitution of $w(r) = w_o$ into Equation (9) and integrating produces

$$(p - p_\infty) = \rho w_o^2 \,[\ln(r) - \ln(d/2)] \tag{11}$$

After substituting Equation (11) into Equation (8) and integrating, the expression becomes

$$G_x = \pi\rho u_o^2 \,(d/2)^2 \,[1 - \frac{1}{2}\,(\frac{w_o}{u_o})^2\,] \tag{12}$$

Finally, putting Equations (10) and (12) into Equation (1) and defining the velocity ratio $F = w_o/u_o$, the swirl number S can be expressed thus:

$$S = \frac{2F/3}{1 - F^2/2} \tag{13}$$

The alternate swirl number S' follows from finding the dynamic axial flux of axial momentum:

$$G_x' = \pi\rho u_o^2 \,(d/2)^2 \tag{14}$$

Using this in Equation (6) leads to the simple expression,

$$S' = 2F/3 \tag{15}$$

By the same procedure, expressions for S and S' for the other four cases are found to be as follows:

For case II with $u(r) = u_o$, $w(r) = w_{mo}\,(\frac{r}{d/2})$, and defining G as w_{mo}/u_o:

$$S = \frac{G/2}{1 - G^2/4} \tag{16}$$

and

$$S' = G/2 \tag{17}$$

For case III with $u(r) = u_{mo}\ (\frac{r}{d/2})$, $w(r) = w_{mo}(\frac{r}{d/2})$, and defining H as w_{mo}/u_{mo}:

$$S = \frac{4H/5}{1 - H^2/2} \tag{18}$$

and

$$S' = 4H/5 \tag{19}$$

For case IV with $u(r) = u_{mo}(\frac{r}{d/2})$, $w(r) = w_{mo}(\frac{r}{d/2})^2$, and defining I as w_{mo}/u_{mo}:

$$S = \frac{I}{1 - 3I^2/4} \tag{20}$$

and

$$S' = I \tag{21}$$

Finally, for case V with $u(r) = u_{mo}\ (\frac{r}{d/2})^2$, $w(r) = w_{mo}\ (\frac{r}{d/2})^2$, and defining J as w_{mo}/u_{mo}:

$$S = \frac{4J/7}{1 - 2J^2/3} \tag{22}$$

and

$$S' = 4J/7 \tag{23}$$

Each of these expressions for S and S' may be inverted to yield the velocity ratio as a function of swirl number. A summary of the inverse relations follows:

Case I -

$$F = \frac{-4/(3S) + [4/(3S)]^2 + 8}{2}$$

$$F = 3S'/2$$

Case II -

$$G = \frac{-2/(S) + [2/(S)]^2 + 16}{2}$$

$$G = 2S'$$

Case III -

$$H = \frac{-8/(5S) + [8/(5S)]^2 + 8}{2}$$

$$H = 5S'/4$$

Case IV -

$$I = \frac{-4/(3S) + [4/(3S)]^2 + 16/3}{2}$$

$$I = S'$$

Case V -

$$J = \frac{-6/(7S) + [6/(7S)]^2 + 6}{2}$$

$$J = 7S'/4$$

Numerical values from each of these expressions are given in Table I, and the same relationships are shown graphically in Fig. 2 for a range of commonly-encountered swirl numbers.

It is evident from the equations alone that the S' expressions are all simple linear relations. The parameters F through J will increase without bound as the swirl number is increased in each case. In contrast, the parameter variation with S shows asymptotic behavior; the exit velocity ratios all approach definite values as swirl number increases. The asymptotic values are also given in Table I.

Although the curves are generally similar in shape, some observations can be made. The curves for cases II and IV are the upper and lower extremes for both the S and S' relations, with the curves for cases I, III, and V falling in between. This may be anticipated since the w profile is of higher order than the u profile for case II (that is, linear versus constant) and the opposite is true for case IV (linear versus parabolic). In the other three cases the u and w profiles are of the same order.

In appraising the usefulness of the idealized profiles, comparison may be made with the measured profiles given later in Chapter IV. As the swirl strength increases from 0 to 70 deg., corresponding profiles of cases I to V appear roughly appropriate. The moderate swirl case (ϕ = 45 deg.) gives the best match with its corresponding idealization (case III, linear axial and swirl profiles), by visual inspection alone. However, the presence of the hub and central recirculation zone prevent adequate representation by the idealized profiles, as demonstrated by the experimental results discussed in Chapter IV.

CHAPTER III

EXPERIMENTAL EQUIPMENT AND PROCEDURE

3.1 Combustor Flowfield Facility

The installation on which all tests were performed is a low-speed wind tunnel designed and built at Oklahoma State University. It produces uniform flow of relatively low turbulence intensity, with continuously adjustable flow rate. The facility consists of a filtered intake, an axial blower, a stilling chamber, a turbulence management section, and a contoured outlet nozzle. A schematic of the facility is shown in Fig. 2.

The intake consists of a rounded entrance containing fixed inlet guide vanes, surrounded by a coarse-mesh screen box covered with foam rubber panels to filter the incoming ambient air. The blower is a six-bladed propeller-type fan, driven by a 5 h.p. U.S. Varidrive motor which can be continuously varied from 1600 to 3100 rpm.

Air from the blower is expanded into the stilling chamber and passes through several fine mesh screens to help remove the turbulence generated by the blower. The turbulence level is further reduced by passage through the turbulence management section. This section, a round duct of 76 cm diameter, contains a perforated aluminum plate (2 mm diameter holes) followed by a fine mesh screen, a section of packed straws 12.7 cm long, and five more fine mesh screens. Most of the turbulence reduction occurs in this section, and any traces of fan-induced swirl are effectively removed by the straws.

To reduce the duct diameter down to the 15 cm outlet diameter, a specially contoured nozzle is used. This was designed after the method of Morel (18) to minimize boundary layer growth and produce a uniform top-hat profile, with no separation or instabilities upstream. The nozzle is of molded fiberglass with a steel flange at the outlet for the attachment of various test articles. A 1 cm diameter hole a short distance upstream of the outlet allows for insertion of a standard pitot-static probe to measure the dynamic pressure upstream of the swirler. This measurement, with a small correction for difference in flow area, is used to calculate the swirler inlet reference velocity, u_{in}.

3.2 Swirler

The swirler used in this study is annular with hub and housing diameters of 3.75 and 15.0 cm respectively, giving a hub-to-swirler diameter ratio z of 0.25. The hub has a streamlined parabolic nose facing upstream and a blunt base (corner radius approximately 2 mm) facing downstream. It is supported by four thin rectangular-section struts or spider arms from the housing wall. The base of the hub protrudes approximately 3 mm downstream of the swirler exit plane. Photographs are schematics of the swirler are shown in Figures 3 through 5.

The ten vanes or blades are attached to shafts which pass through the housing wall and allow individual adjustment of each blade's angle. The standard vanes are wedge-shaped for nearly-constant pitch-to-chord ratio σ of approximately 0.68, which according to two-dimensional cascade data should give good flow-turning effectiveness. Sets of vanes with chord widths of 0.5 and 0.75 of the standard width may be installed to study the effect of increased pitch-to-chord ratio on turning effectiveness, nonaxisymmetry, and radial secondary flow patterns. Vane planforms are shown in Figure 6.

3.3 Five-Hole Pitot Probe and Instrumentation

Velocity profile measurements were made using a five-hole pitot probe (Model DC-125-12-CD by United Sensor Division of United Electrical Controls Co.), one of the few instruments capable of measuring the magnitude and direction of the local time-mean velocity vector simultaneously. Detailed explanations of five-hole pitot operating techniques and basic principles may be found in Reference 5. A schematic of the probe tip geometry showing the velocities and angles measured is given in Figure 7.

The probe is mounted in a traversing mechanism (Model C1000-12 from United Sensor) which in turn is mounted on a 30-cm diameter plexiglass tube which fits closely over the swirler exit flange. This tube comprises the test section for combustor flowfield modeling in related studies (1-10) and creates confined-jet conditions downstream of the swirler. The presence of the test section tube has negligible effect on the flow patterns observed at the swirler exit plane.

The traversing mechanism allows the probe to be translated vertically (on a radial line outward from the test section axis) and rotated 360 degrees about the probe's yaw axis. In addition to the motion permitted by the traverse mechanism, the test section tube on which the traverse mechanism is mounted may be rotated about its axis with respect to the swirler, thereby allowing azimuthal traverses to be performed.

Tubing from the probe's five pressure taps is routed through selector valves so that pressure differences between any two of the probe's five holes may be measured by a differential pressure transducer (Type 590 Barocel Pressure Sensor by Datametrics Inc., ± 10 torr range). The resulting pressure difference values are then read directly from a digital voltmeter with selectable averaging time-constant (Model 1076 True RMS Voltmeter by TSI, Inc.).

3.4 Calibration, Measurement, and Reduction Procedure

Calibration of the five-hole probe is done using a small free jet which has a contoured nozzle similar to that of the flowfield facility. The probe tip is placed in the uniform parallel flow of the jet potential core and adjusted to zero yaw angle. The probe is then rotated about its pitch axis and values of $(p_N - p_S)$, $(p_C - p_W)$, and $(p_C - p_{atm})$ pressure differences are measured at different values of pitch angle δ.

Velocity measurements with the five-hole probe are made after the probe has been carefully aligned with the facility and the pressure transducer properly zeroed. At each measurement location, the probe is aligned with the local flow direction in the horizontal plane by nulling the pressure difference $(p_E - p_W)$. The value of yaw angle β is then read from the rotary vernier on the traverse mechanism. Finally, values of the pressure differences $(p_N - p_S)$, $(p_C - p_W)$, and $(p_C - p_{atm})$ are measured.

The raw pressure data are reduced by a computer program to yield nondimensionalized values of the u, v, and w velocity components, as well as the static pressure at each location. The reduction program also performs numerical integration on the radial traverses to obtain values of the axial and angular momentum fluxes, and from these calculates the swirl numbers S and S'. Some details of the reduction procedure are given in Appendix C, the description of changes made to the reduction code, while more general descriptions of the original code are found in references (19) and (20). A listing of the code with sample input and output is given in Appendix D.

CHAPTER IV

EXPERIMENTAL RESULTS

Velocity profiles from both radial and azimuthal traverses for each of the flowfields investigated are now presented and discussed.

Table II gives a summary of the operating conditions used during the studies. With nonswirling conditions, the low fan speed delivers relatively high axial velocity and corresponding Reynolds number. At progressively higher swirl strength conditions, progressively higher fan speeds are used, but even so exit velocities and Reynolds numbers reduce because of increasing flow restriction of the swirler. However, based on a limited study elsewhere (4), it is expected that all flowfields are in the Reynolds number independent regime.

The radial traverses consist of ten points from the centerline to the swirler exit radius, spaced 7.6 mm apart. Of these ten, only seven stations were actually measured since the hub blocked the inner three positions. The azimuthal traverses contain nine points spaced 6 degrees apart at a constant radial distance from the centerline. Azimuth angles θ were taken from -24 to +24 degrees, with the $\theta = 0$ position in line with the shaft of one of the swirl vanes. A diagram showing the traverse patterns on the face of the swirler is given in Figure 8.

Unless otherwise stated all traverses are taken immediately after the swirler exit downstream face with no expansion blocks present. Nominally, this location is $x/D = -0.109$, where the positon $x/D = 0.0$

is the expansion station, separated from the swirler in practice (5-10) with one of the expansion blocks. Only for the data presented in Tables XV and XVI and Figures 21 and 22 is the expansion block affixed to the downstream face of the swirler and measurements then taken at x/D = 0.0.

4.1 Velocity Profiles From Radial Traverses

Axial, radial and swirl velocity component data are tabulated in Tables III through VIII for radial traverses from the swirler centerline to the swirler exit radius. Data are presented for five values of swirl blade angle: zero (no swirler), zero (with swirler), 38, 45, 60, and 70 deg. Corresponding velocity profile plots are shown in Figure 9 to 14, with the profiles extending from the centerline to twice the exit radius (r/D = 0.5 where D is the test section diameter used in associated studies). All velocities shown are normalized with respect to the swirler inlet uniform axial velocity, deduced independently from the pitot-static measurement upstream of the swirler. The outer ten data points are zero in each profile because the presence of the solid boundary of the swirler flange precluded measurements at these locations.

The nonswirling case shown in Fig. 9 has a nearly-flat axial velocity profile, as expected for the plain nozzle opening without the swirler installed. There is no measurable swirl velocity, and the radial velocity is zero except for points very near the edge of the exit, where the flow begins to anticipate the abrupt expansion to twice the exit diameter. The second nonswirling case, see Figure 10, has the swirler installed with the blades set to ϕ = 0 deg. The traverse was made midway between two blades and away from any of the hub supporting struts. Here again the axial profile is quite flat, with just a slight increase toward the hub. However, the velocity has increased by nearly 25 percent, because of the decrease in flow area with swirler hub and vanes in place. In addition, the hub induces a negative radial velocity across the entire annulus, overriding the tendency to anticipate the expansion corner. The swirl velocity is, as expected, negligible.

The 38-degree blade-angle case in Figure 11 shows remnants of the flat inlet profile over a small portion of the radius near the outside edge in both the axial and swirl profiles. The presence of the hub now constrains the three innermost points to zero, and the region between the hub and the flat portion in the axial and swirl profiles is approximately linear. The maximum axial velocity is 1.5 times the inlet axial velocity because the flow area is decreased by the hub and also because centrifugal effects have shifted the profile outward. The radial velocity has an irregular profile with a maximum value of one-half the inlet axial velocity.

In the ϕ = 45 degree case of Figure 12 the flat segments are no longer present and both axial and swirl profiles vary from zero at the hub to a maximum at or near the rim of the swirler in an almost linear fashion. The similar shape and magnitude of the profiles indicates that the turning angle is fairly uniform and only slightly less than 45 degrees. The radial velocity is again irregular, but shows a step at r/D = 0.1 similar to that in the axial and swirl profiles; this is probably due to the central recirculation zone downstream beginning to slow down the flow upstream of it.

Profiles ensuing from the case of ϕ = 60 degrees, see Figure 13, all have a sharply peaked shape, with most of the flow leaving near the outer boundary. The radial component is considerably stronger, with a peak value nearly twice that of the reference velocity upstream of the swirler. The step in the 45 degree axial profile has now developed into reverse flow, indicating that the central recirculation zone now extends upstream past the exit plane. The reverse flow is accompanied by reduced swirl velocity and very low values of radial velocity. The positive axial velocity adjacent to the hub may be the result of a slight clearance between the blades and the hub, allowing air with greater axial momentum to pass through.

Exit velocity profiles obtained for the strongest swirl case considered (ϕ = 70 deg.) are shown in Figure 14. Almost all of the flow leaves the swirler at the outside edge. The maximum axial and swirl velocities are approximately 3 and 2.5 times the upstream reference values, respectively, and the velocity gradients across the profiles are quite large. The reverse flow in the center of the axial profile is stronger than in the 60-degree case and is now accompanied by negative or inward radial velocity. This suggests the possibility of a vortex ring structure occurring at the exit of the swirler under high-swirl conditions. The swirl velocity profile remains positive but shows a step corresponding to the outer boundary of the recirculation zone.

4.2 Velocity Profiles from Azimuthal Traverses

An indication of the azimuthal or θ-variation of axial, radial, and swirl velocities is now given for the same vane angle settings used in the radial traverses. The measurements were taken at a constant radial position of $r/D = 0.179$, which in most cases illustrates adequately the azimuthal flow variation. However, measurements at r/D = 0.204 were necessary in the ϕ = 70 degree case to get data more representative of the main region of the flow. In addition, azimuthal traverse measurements were taken 0.109 D downstream (at $x/D = 0.0$, expansion corner with the 90-degree block installed) for $\phi = 70$ degrees to investigate further the upstream extent of the central recirculation zone. Radial profiles at this location for all degrees of swirl are already available (3).

Measurements in each case span an angle of 48 degrees, somewhat more than the 36 degrees between successive blades. Data are tabulated in numerical form in Tables IX through XVI, and corresponding velocity profiles are given in Figures 15 through 22.

The variations in all normalized velocity components u, v, and w occur in approximately 36-degree cycles, coinciding with the blade spacing. The profiles all show significant variation with azimuthal position, except for those in or near recirculation zones where the w velocity component is dominant. These variations can be attributed to several causes, among them being blade stall from using flat blades at high angles of attack and wakes from blunt trailing edges.

Figure 15 shows the azimuthal profile with the swirler installed, but with the vanes set to zero angle. The $\theta = 0$ degree position is directly downstream of one of the swirl vanes, approximately 3 mm from the trailing edge at the $r/d = 0.179$ position. The velocity defect in the wake of the blade is clearly seen in the axial velocity profile, although the precise accuracy of these measurements is uncertain because of the velocity gradients across the width of the probe. The decreased u-velocity at the left side of the profile is caused by the presence of an upstream strut supporting the hub, located at $\theta = +24$ degrees. The radial velocity is uniformly negative indicating inflow over most of the range, which agrees well with the results of the radial traverse shown earlier in Figure 10. The radial velocity is positive only in the blade wake region. The swirl velocity, as expected, is effectively zero.

Figure 16 presents the results of an azimuthal traverse for the ϕ = 38 degrees low-swirl case. The measurement position at r/D = 0.179 is in the middle of the flat portion of the radial profile, as may be deduced from observation of Figure 3. The 36-degree cyclic variation from one blade to the next is apparent in each of the profiles. The u and w profiles have a flat portion, apparently between blade wakes, with an average yaw angle of about 39 degrees. This confirms the assumption that the blade pitch/chord ratio of 0.68 is sufficient to adequately turn the flow. In fact, over the rest of the profile, the turning angle is even higher than the blade angle ϕ. The radial velocity shows no flat region and varies the most of the three components. It is also quite large even at this low degree of swirl.

In the case of ϕ = 45 degrees, Figure 17 illustrates that the 36-degree cycle is not as clear, but nevertheless significant variation exists in all profiles. The radial component is nearly as large as the axial and swirl components in some places, and again exhibits the greatest variation with azimuthal position.

For the 60-degree swirl case of Figure 18 variations with azimuthal position are again evident in all profiles. The variation is less than in the cases seen heretofore, possibly because the main flow has shifted further outward under centrifugal effects and the measurement position is in a region of reduced velocity.

This effect is even more notable in the ϕ = 70 degrees profiles portrayed in Figure 19. The measurement position is now no longer in the main exiting flow, but on the edge of the central recirculation zone. The axial velocity here is effectively zero, although considerable swirl and radial velocities are present. The radial velocity, it should be noted, is negative or inward towards the centerline. Azimuthal variations are fairly small here, which is to be expected since the flow is mainly in the azimuthal direction. To get a more representative sample of the exiting flow from the swirler with blades at 70 degrees a traverse was made at the next outward radial station at r/D = 0.204. When the velocity profiles shown in Figure 20 are compared with those in the previous figure, the effects of extreme velocity gradients in the radial direction may be perceived. The accuracy of the radial velocity and pitch angle measurements may be suspect in the presence of high radial velocity gradients, but the major features of the flow can still be assessed. In a radial distance of only 7.6 mm, the axial velocity jumps from zero to over 12 m/s. In addition, the swirl velocity increases over 50 percent and the radial velocity changes sign. The 36-degree cyclic variation with blade spacing is again present in all profiles.

To investigate further the complexities of the flow with swirl vane angle ϕ = 70 degrees, azimuthal traverses were also made 3.25 cm downstream of the location of measurements just discussed. Both radial locations, r/D = 0.179 and 0.204, were investigated at x/D = 0.0. This is the axial location of the expansion station in practice, (1,3,5, 7-9) and the 90 degree expansion block was affixed to the downstream face of the swirler for these measurements. The profiles appear in Figures 21 and 22; they may be compared with corresponding profiles from further upstream in Figures 19 and 20, respectively. It appears from both sets of profiles that the recirculation zone has narrowed somewhat with the additional length before the expansion corner. At the inner radial position ($r/D = 0.179$) of Figure 21, the axial velocity is no longer zero. It is now positive, indicating that the main exit flow has moved slightly further inward. The azimuthal variation is still quite small, however, suggesting that the damping influence of the recirculation zone is still in effect. At the outer radial position ($r/D = 0.204$) of Figure 22 the axial and radial velocities are larger than at the upstream position, also implying that the outer high-velocity zone has moved further inward. The azimuthal variation is again similar to that of the exit-plane position at the same radius.

4.3 Calibration Sensitivity Verification

Since minor variations occur from one probe calibration to the next, it was decided to check the sensitivity of the data reduction procedure to these variations. The case of swirl vane angle $\phi = 70$ degrees was used, at $x/D = -0.109$ and $r/D = 0.179$. The most recent calibration provided the baseline values of the pitch and velocity coefficients, (5,7) which were then varied by increasing the magnitude of each value by ten percent. Three cases were tried: increased pitch coefficient with baseline velocity coefficient, increased velocity coefficient with baseline pitch coefficient, and increased values of both coefficients. The percent difference in the output values of the velocity components is shown in Tables XVII through XIX for each of these three cases respectively.

Referring to Table XVII, changing the pitch coefficient value is seen to affect the radial component the most, as expected. The change in output stays below ten percent for all but three of the output values. For the case of increased velocity coefficient only, Table XVIII shows a quite uniform increase of less than five percent over all the values. This indicates a relatively predictable, low sensitivity response to changes in the calibration velocity coefficient.

The final case, shown in Table XIX, indicates that increases in both coefficients tend to cancel each other for the radial velocity measurement, which was the most sensitive to pitch coefficient variation. The axial and swirl components increase somewhat, but all variations remain well below ten percent. This relative insensitivity to calibration errors is satisfying but it should be noted if the coefficient changes are of opposite sign in the combined case, errors of greater than ten percent in the radial velocity measurements would probably ensue.

4.4 Swirl Strength Comparison

For comparison with the results of the idealized profile derivations, swirl numbers S and S' were calculated from experimental data using Equations (1) and (6) with the turbulent stress terms omitted. Measured velocities and pressures from the radial traverses described in Section 4.1 were used, with appropriate numerical integration performed by the computer data reduction program described in Appendixes C and D. Since actual wall static pressure measurements were unavailable, the reference pressure P_∞ was taken as the static pressure measurement at $r/D = 0.230$, the point nearest the outer edge of the swirler. The results are given in Table XX, showing the asymptotic behavior of the flat swirl vanes in producing strong swirl. Also shown in Table XX is the ratio w_{mo}/u_{mo} for each vane angle, taken from the measured radial traverse data. These ratios were used to compare the actual profiles with the idealized ones.

Two comparisons were made to investigate the usefulness of the idealized profiles. In the first, swirl numbers from the measured profiles were compared with those predicted by the Case I idealization. This was done by making the standard assumption that an "ideal" flat-blade swirler (with an infinite number of infinitely thin blades) operating on a plug flow would produce flat exit profiles as shown in Figure 1, part (a). The flow turning angle would be everywhere equal to the vane angle ϕ, and the ratio $w_o/u_o = F$ would be equal to tan ϕ. Corresponding S and S' values for each vane angle are then found using Equations (13) and (15) or Figure 2 with F = tan ϕ. The results for the four swirl vane angles used are shown in the left half of Table XXI. It is immediately apparent that the negative S values for ϕ = 60 and 70 degrees are based on values of F greater than the asymptotic value, and are physically unrealistic. The S values for ϕ = 38 and 45 degrees are considerably higher than the measured values, while the S' values start close to the measured ones but diverge rapidly at high vane angles. This confirms the unsuitability of the Case I idealization for modeling flat-bladed swirler performance.

The other comparison was done using the "most appropriate" idealized case, as judged by visual comparison of the profile shapes. The measured value of the ratio of maximum profile velocities from Table XX was used instead the tan ϕ assumption, which has no theoretical basis for Cases II-V. Most appropriate cases were determined to be Case I for ϕ = 38, Case III for ϕ = 45, and Case V for ϕ = 60 and 70 degrees. S and S' values were then determined using Equations (13) and (15), (18) and (19), and (22) and (23). Results are shown in the right-hand side of Table XXI. Again we see considerable discrepancies between the actual and idealized values for both S and S'. Although use of Cases III and V gives a much better match for the higher swirl vane angles, the newer idealized profiles are still inappropriate for modeling actual swirler output. The disparities may be attributed to the presence of the central hub, the upstream extent of the central recirculation zone, and flat swirl-vane ineffectiveness at high angles of attack, with associated wakes and nonaxisymmetries.

CHAPTER V

CLOSURE

5.1 Summary and Conclusions

This study has investigated the performance characteristics of an axial vane-type swirler, used in combustor flowfield measurements and turbulence modeling research. A theoretical analysis of swirl numbers associated with several idealized exit velocity profiles is included, and values of the ratio of maximum swirl velocity to maximum axial velocity at different swirl numbers are tabulated for each case. Measurements of actual swirler exit velocity profiles were made for swirl vane angles ϕ = 0, 38, 45, 60, and 70 degrees using a five-hole pitot probe technique. The values of normalized velocity components are tabulated and plotted as part of the data base for the evaluation of flowfield prediction codes and turbulence models.

Assumptions of flat axial and swirl profiles with radial velocity equal to zero were found to be progressively less realistic as the swirler blade angle increases. At low swirl strengths (ϕ = 38), portions of the u and w profiles remain flat while the v-component is already significant. At moderate swirl ϕ = 45 degrees, approximately linear profiles of u and w with radius are found, with strong v velocity. At stronger swirl ϕ = 60 degrees, even more spiked profiles are seen with most of the flow leaving the swirler near its outer edge, and some reverse flow near the hub. At strong swirl ϕ = 70 degrees, the profiles are extremely spiked with flow reversal. The central recirculation zone extends upstream of the exit plane, almost to the swirler blades in high-swirl cases. Because of this recirculation and the presence of the hub, none of the idealizations considered could model actual swirl cases adequately.

The flow-turning effectiveness of the flat blades was generally adequate for all vane angles tested. However, the large variations of flow angles and velocities with radius made meaningful comparisons with two-dimensional cascade data impossible. Nonaxisymmetry was found in all swirl cases investigated.

5.2 Recommendations for Further Work

Other aspects of swirler performance not covered by this project include pressure drop across the swirler and the efficiency of swirl generation. It is recommended that these be investigated for the present swirler to allow comparison with values quoted by other swirl researchers.

Development of idealized profiles accounting for annular flow and recirculation is another area in which further work is recommended. This should include relating the ratios at maximum profile velocities to effective vane angles to allow prediction of swirler output for a given vane angle setting.

Finally, it is suggested that an uncertainty analysis be done on the five-hole pitot technique to estimate the effects of turbulence intensity and velocity gradients on the accuracy of measurement results.

ORIGINAL PAGE IS
OF POOR QUALITY

REFERENCES

(1) Lilley, D. G., and Rhode, D. L., A Computer Code for swirling Turbulent Axisymmetric Recirculation Flows in Practical Isothermal Combustor Geometries, NASA CR-3442, Feb. 1982.

(2) Rhode, D. L., Lilley, D. G., and McLaughlin, D. K., On the Prediction of Swirling Flowfields Found in Axisymmetric Combustor Geometries. ASME Journal of Fluids Engng., Vol. 104, 1982, pp. 378-384.

(3) Sander, G. F., Annular Vane Swirler Performance. Proceedings, Thirteenth Southwestern Graduate Research Conference in Applied Mechanics, Norman, Oklahoma, April 16-17, 1982, pp. 274-278.

(4) Abujelala, M. T., and Lilley, D. G., Confined Swirling Flow Predictions, Paper AIAA-83-0316, Reno, Nevada, Jan. 10-13, 1983.

(5) Rhode, D. L., Lilley, D. G., and McLaughlin, D. K., Mean Flowfields in Axisymmetric Combustor Geometries with Swirl, Paper AIAA 82-0177, Orlando, Florida, Jan. 11-14, 1982. AIAA Journal, 1983 (in press).

(6) Lilley, D. G., Turbulent Combustor Flowfield Investigation. Paper in Combustion Fundamentals Research Conference, held at NASA Lewis Research Center, Cleveland, Ohio, Oct. 21-22, 1982, pp. 152-168.

(7) Yoon, H. K., and Lilley, D, G., Five-Hole Pitot Probe Time-Mean Velocity Measurements in Confined Swirling Flows. Paper AIAA-83-0315, Reno, Nevada, January 10-13, 1983.

(8) Janjua, S. I., McLaughlin, D. K., Jackson, T. W., and Lilley, D. G., Turbulence Measurements in a Confined Jet Using a Six Orientation Hot-Wire Probe Technique, Paper AIAA 82-1262, Cleveland, Ohio, June 21-23, 1982.

(9) Jackson, T. W., and Lilley, D. G., Swirl Flow Turbulence Measurements Using a Single-Wire Technique. Paper AIAA-83-1202, Seattle, Wash., June 27-29, 1983.

(10) Janjua, S. I., and McLaughlin, D. K., Turbulence Measurements in a Swirling Confined Jet Flowfield Using a Triple Hot-Wire Probe. Report DT-8178-02, Dynamics Technology, Inc., Torrance, CA, Nov. 1982.

ORIGINAL PAGE IS
OF POOR QUALITY

(11) Kerr, N. M., and Fraser, D., Swirl. Part I: Effect on Axisymmetrical Turbulent Jets. Journal of the Inst. of Fuel, Vol. 38, Dec. 1965, pp. 519-526.

(12) Mathur, M. L., and MacCallum, N. R. L., Swirling Air Jets Issuing from Vane Swirlers. Part I: Free Jets; Part II: Enclosed Jets. Journal of the Inst. of Fuel, Vol. 40, May 1967, pp. 214-245.

(13) Chigier, N. A. and Chervinsky, A., Experimental Investigation of Swirling Vortex Motion in Jets. Journal of Applied Mechanics, Vol. 34, June 1967, pp. 443-451.

(14) Beer, J. M., and Chigier, N. A., Combustion Aerodynamics. Applied Science Publishers, London, 1972.

(15) Beltagui, S. A., and MacCallum, N. R. L., Aerodynamics of Vane-Swirled Flames in Furnaces. Journal of the Inst. of Fuel, Vol. 49, Dec. 1976, pp. 183-193.

(16) Gupta, A. K., and Lilley, D. G., Flowfield Modeling and Diagnostics. Abacus Press, Tunbridge Wells, England, 1983 (in press).

(17) Beltagui, S. A., and MacCallum, N. R. L., The Modelling of Vane-Swirled Flames in Furnaces. Journal of the Inst. of Fuel, Vol. 40, Dec. 1976, pp. 193-200.

(18) Morel, T., Comprehensive Design of Axisymmetric Wind Tunnel Contractions. Paper ASME 75-FE-17, Minneapolis, Minnesota, May 5-7, 1975.

(19) Rhode, D. L., "Predictions and Measurements of Isothermal Flowfields in Axisymmetric Combustor Geometries," Ph.D. Thesis, Dept. of Mechanical and Aerospace Engineering, Oklahoma State University, Dec. 1981.

(20) Yoon, H. K., "Five-Hole Pitot Probe Time-Mean Velocity Measurements in Confined Swirling Flows," M.S. Thesis, Dept. of Mechanical and Aerospace Engineering, Oklahoma State University, July 1982.

(21) Bryer, D. W., and Pankhurst, R. C., Pressure-Probe Methods for Determining Wind Speed and Flow Direction. Her Majesty's Stationery Office, London, 1971.

(22) Lilley, D. G., and Rhode, D. L., "A Computer Code for Swirling Turbulent Axisymmetric Recirculating Flows in Practical Isothermal Combustor Geometries," Report NASA CR-3442, NASA Lewis Research Center, Cleveland, Ohio, Feb. 1982.

APPENDIX A

TABLES

TABLE I

RATIOS OF MAXIMUM SWIRL AND AXIAL VELOCITIES F-J OF IDEALIZED PROFILE CASES I - V, FOR COMMON VALUES OF SWIRL NUMBERS S AND S'

S	F	S'	F
0.10	0.148	0.10	0.150
0.25	0.352	0.25	0.375
0.50	0.610	0.50	0.750
0.75	0.782	0.75	1.125
1.00	0.897	1.00	1.500
1.50	1.038	1.50	2.250
2.00	1.120	2.00	3.000
∞	1.414	∞	∞

(a) Case I - Flat axial and swirl profiles, $F = w_o/u_o$

TABLE I (Continued)

S	G	S'	G
0.10	0.198	0.10	0.200
0.25	0.472	0.25	0.500
0.50	0.828	0.50	1.000
0.75	1.070	0.75	1.500
1.00	2.236	1.00	2.000
1.50	1.442	1.50	3.000
2.00	1.562	2.00	4.000
∞	2.000	∞	∞

(b) Case II - Flat axial and linear swirl profiles, $G = w_o/u_{mo}$

TABLE I (Continued)

S	H	S'	H
0.10	0.124	0.10	0.125
0.25	0.299	0.25	0.313
0.50	0.535	0.50	0.625
0.75	0.705	0.75	0.938
1.00	0.825	1.00	1.250
1.50	0.978	1.50	1.875
2.00	1.070	2.00	2.500
∞	1.414	∞	∞

(c) Case III - Linear axial and swirl profiles, $H = w_{mo}/u_{mo}$

TABLE I (Continued)

S	I	S'	I
0.10	0.099	0.10	0.100
0.25	0.239	0.25	0.250
0.50	0.431	0.50	0.50
0.75	0.568	0.75	0.750
1.00	0.667	1.00	1.000
1.50	0.793	1.50	1.500
2.00	0.869	2.00	2.000
∞	1.155	∞	∞

(d) Case IV - Parabolic axial and linear swirl profiles, $I = w_{mo}/u_{mo}$

TABLE I (Continued)

S	J	S'	J
0.10	0.172	0.10	0.175
0.25	0.393	0.25	0.438
0.50	0.638	0.50	0.875
0.75	0.780	0.75	1.313
1.00	0.869	1.00	1.750
1.50	0.972	1.50	2.625
2.00	1.029	2.00	3.500
∞	1.225	∞	∞

(e) Case V - Parabolic axial and swirl profiles, $J = w_{mo}/u_{mo}$

TABLE II

SUMMARY OF OPERATING CONDITIONS

ϕ (degrees)	FS (rpm)	u_{in} (m/s)	$Re_d \times 10^{-5}$
0	1950	23.00	2.22
38	2265	13.30	1.30
45	2600	13.00	1.26
60	2800	9.20	0.90
70	2800	5.52	0.53

* Abbreviations used are:

ϕ Swirl vane angle

FS Fan speed

u_{in} Spatial-mean swirler exit axial velocity, deduced from independent upstream measurement, excluding presence of the hub and swirler

Re_d Swirler-exit Reynolds number based on u_{in} and swirler diameter

TABLE III

NORMALIZED VELOCITY COMPONENTS, YAW ANGLE, PITCH ANGLE, AND STATIC PRESSURE DIFFERENCE ($p-p_\infty$) FROM RADIAL TRAVERSE, ϕ = 0 DEG.
(NO SWIRLER)

J	R/D	U/UIN	V/UIN	W/UIN	BETA	DELTA	P-PREF
10	0.230	1.025	0.058	-0.000	360.0	3.3	0.00
9	0.204	1.011	0.038	-0.000	360.0	2.1	11.[illegible]2
8	0.179	1.001	0.020	-0.000	360.0	1.1	18.46
7	0.153	0.997	0.010	-0.000	360.0	0.6	21.07
6	0.128	0.996	0.008	-0.000	360.0	0.4	21.33
5	0.102	0.997	0.006	-0.000	350.0	0.3	21.93
4	0.077	0.997	0.011	-0.000	360.0	0.7	21.65
3	0.051	0.996	0.017	-0.000	360.0	1.0	0.00
2	0.026	0.995	0.021	-0.000	360.0	1.2	0.00
1	0.000	0.995	0.022	-0.000	360.0	1.3	0.00

ORIGINAL PAGE IS
OF POOR QUALITY

TABLE IV

NORMALIZED VELOCITY COMPONENTS, YAW ANGLE, PITCH ANGLE, AND STATIC PRESSURE DIFFERENCE ($p-p_\infty$) FROM RADIAL TRAVERSE, ϕ = 0 DEG. (SWIRLER INSTALLED)

J	R/D	U/UIN	V/UIN	W/UIN	BETA	DELTA	P-PREF
10	0.230	1.219	-0.019	0 000	0.0	-0.9	0 00
9	0.204	1.204	-0.046	-0.006	-0.3	-2.2	9.74
8	0.179	1.210	-0.063	0.000	0.0	-3.0	5.87
7	0.153	1.209	-0.073	-0.002	-0.1	-3.4	6.66
6	0.128	1.203	-0.091	-0.004	-0.2	-4.3	8.15
5	0.102	1.214	-0.092	0.002	0.1	-4.3	1.97
4	0.077	1.220	-0.102	0.011	0.5	-4.8	-6.51
3	0.051	0.000	0.000	0.000	0.0	0.0	0.00
2	0.026	0.000	0.000	0.000	0.0	0.0	0.00
1	0.000	0.000	0.000	0.000	0.0	0.0	0.00

TABLE V

NORMALIZED VELOCITY COMPONENTS, YAW ANGLE, PITCH ANGLE, AND STATIC PRESSURE DIFFERENCE $(p-p_\infty)$ FROM RADIAL TRAVERSE, ϕ = 38 DEG.

J	R/D	U/UIN	V/UIN	W/UIN	BETA	DELTA	P-PREF
10	0.230	1.018	0.176	0.751	36.4	7.9	0.00
9	0.204	1.435	0.364	1.145	38.6	11.2	1.78
8	0.179	1.417	0.385	1.139	38.8	11.9	9.09
7	0.153	1.454	0.486	1.112	37.4	14.9	-11.31
6	0.128	1.080	0.352	0.843	38.0	14.4	-17.49
5	0.102	0.817	0.250	0.483	30.6	14.8	-18.95
4	0.077	0.187	0.231	0.251	53.4	36.5	-16.45
3	0.051	0.000	0.000	0.000	0.0	0.0	0.00
2	0.026	0.000	0.000	0.000	0.0	0.0	0.00
1	0.000	0.000	0.000	0.000	0.0	0.0	0.00

TABLE VI

NORMALIZED VELOCITY COMPONENTS, YAW ANGLE, PITCH ANGLE, AND STATIC PRESSURE DIFFERENCE $(p-p_\infty)$ FROM RADIAL TRAVERSE, ϕ = 45 DEG.

J	R/D	U/UIN	V/UIN	W/UIN	BETA	DELTA	P-PREF
10	0.230	1.706	0.584	1.494	41.2	14.4	0.00
9	0.204	1.662	0.522	1.539	42.8	13.0	5.35
8	0.179	1.540	0.541	1.396	42.2	14.6	-19.76
7	0.153	1.089	0.528	0.914	40.0	20.4	-43.66
6	0.128	0.672	0.549	0.632	43.2	30.8	-55.18
5	0.102	0.356	0.343	0.553	57.2	27.5	-56.10
4	0.077	0.351	0.332	[illegible]	29.2	39.5	-51.58
3	0.051	0.000	0.000	0.000	0.0	0.0	0.00
2	0.026	0.000	0.000	0.000	0.0	0.0	0.00
1	0.000	0.000	0.000	0.000	0.0	0.0	0.00

TABLE VII

NORMALIZED VELOCITY COMPONENTS, YAW ANGLE, PITCH ANGLE, AND STATIC PRESSURE DIFFERENCE ($p-p_\infty$) FROM RADIAL TRAVERSE, ϕ = 60 DEG.

J	R/D	U/UIN	V/UIN	W/UIN	BETA	DELTA	P-PREF
10	0.230	2.421	1.698	2 273	43.2	27.1	0.00
9	0.204	1.802	1.420	1.358	37.0	32.2	-14.52
8	0.179	1.312	1.070	0.982	36.8	33.1	-50.38
7	0.153	0.562	0.450	0.833	56.0	24.1	-34.46
6	0.128	-0.087	0.059	0.504	99.8	6.5	-37.27
5	0.102	-0.059	0.096	0.420	98.0	12.7	-40.04
4	0.077	0.546	0.068	0.527	44.0	5.1	-50.51
3	0.051	0.000	0.000	0.000	0.0	0.0	0.00
2	0.026	0.000	0.000	0.000	0.0	0.0	0.00
1	0.000	0.000	0.000	0.000	0.0	0.0	0.00

ORIGINAL PAGE IS
OF POOR QUALITY

TABLE VIII

NORMALIZED VELOCITY COMPONENTS, YAW ANGLE, PITCH ANGLE, AND STATIC PRESSURE DIFFERENCE ($p-p_\infty$) FROM RADIAL TRAVERSE, ϕ = 70 DEG.

J	R/D	U/UIN	V/UIN	W/UIN	BETA	DELTA	P-PREF
10	0.230	3.005	1.547	2.55[illegible]	41.6	22.[illegible]	[illegible]
9	0.204	1.817	0.890	1.514	39.8	18.7	-18.25
8	0.179	0.176	0.034	1.001	80.0	1.9	-21.30
7	0.153	-0.512	-0.131	0.927	117.4	-6.7	-25.30
6	0.128	-0.475	-0.145	0.721	112.4	-9.5	-28.47
5	0.102	-0.152	-0.068	0.424	110.4	-8.5	-31.18
4	0.077	0.731	0.473	0.705	44.0	25.0	-35.11
3	0.051	0.000	0.000	0.000	0.0	0.0	0.00
2	0.026	0.000	0.000	0.000	0.0	0.0	0.00
1	0.000	0.000	0.000	0.000	0.0	0.0	0.00

TABLE IX

NORMALIZED VELOCITY COMPONENTS, YAW ANGLE, PITCH ANGLE, AND STATIC PRESSURE DIFFERENCE ($p-p_\infty$) FROM AZIMUTHAL TRAVERSE, ϕ = 0 DEG. AT r/D = 0.179 (SWIRLER INSTALLED)

K	THETA (DEG.)	U/UIN	V/UIN	W/UIN	BETA	DELTA	P-PREF
1	-24.0	1.196	-0.066	-0.012	-0.6	-3.2	7.83
2	-18.0	1.196	-0.066	0.000	0.0	-3.1	8.60
3	-12.0	1.197	-0.065	0.013	0.6	-3.1	9.84
4	-6.0	1.199	-0.047	0.040	1.9	-2.2	7.20
5	0.0	0.278	0.201	0.002	0.5	35.9	46.01
6	6.0	1.201	-0.049	-0.042	-2.0	-2.4	8.12
7	12.0	1.201	-0.060	-0.010	-0.5	-2.9	8.85
8	18.0	1.174	-0.059	0.012	0.6	-2.9	8.20
9	24.0	0.992	-0.075	0.031	1.8	-4.3	12.15

TABLE X

NORMALIZED VELOCITY COMPONENTS, YAW ANGLE, PITCH ANGLE, AND STATIC PRESSURE DIFFERENCE ($p-p_\infty$) FROM AZIMUTHAL TRAVERSE, ϕ = 38 DEG. AT r/D = 0.179

K	THETA (DEG.)	U/UIN	V/UIN	W/UIN	BETA	DELTA	P-PREF
1	-24.0	1.342	0.637	1.187	41.5	19.6	-16.93
2	-18.0	1.236	0.453	1.067	40.8	15.5	2.72
3	-12.0	1.153	0.171	0.971	40.1	6.5	17.41
4	-6.0	1.488	0.184	1.192	38.7	5.5	0.95
5	0.0	1.486	0.307	1.186	38.6	9.2	0.02
6	6.0	1.458	0.419	1.189	39.2	12.6	1.75
7	12.0	1.408	0.536	1.228	41.1	16.0	-7.77
8	18.0	1.288	0.523	1.100	40.5	17.2	1.99
9	24.0	1.141	0.172	1.003	41.3	6.5	19.69

TABLE XI

NORMALIZED VELOCITY COMPONENTS, YAW ANGLE, PITCH ANGLE, AND STATIC PRESSURE DIFFERENCE ($p-p_\infty$) FROM AZIMUTHAL TRAVERSE, ϕ = 45 DEG. AT r/D = 0.179

K	THETA (DEG.)	U/UIN	V/UIN	W/UIN	BETA	DELTA	P-PREF
1	-24.0	1.770	0.864	1.495	40.2	20.5	0.95
2	-18.0	1.683	1.175	1.443	40.6	27.9	4.71
3	-12.0	1.602	1.137	1.344	40.0	28.5	6.13
4	-6.0	1.473	0.530	1.402	43.6	14.6	1.79
5	0.0	1.658	0.416	1.579	43.6	10.3	-4.27
6	6.0	1.759	0.594	1.617	42.6	14.0	-8.37
7	12.0	1.721	0.828	1.616	43.2	19.3	-14.20
8	18.0	1.582	1.132	1.527	44.0	27.2	-22.61
9	24.0	1.201	0.764	1.059	41.4	25.5	-11.50

TABLE XII

NORMALIZED VELOCITY COMPONENTS, YAW ANGLE, PITCH ANGLE, AND STATIC PRESSURE DIFFERENCE ($p-p_\infty$) FROM AZIMUTHAL TRAVERSE, ϕ = 60 DEG. AT r/D = 0.179

K	THETA (DEG.)	U/UIN	V/UIN	W/UIN	BETA	DELTA	P-PREF
1	-24.0	1.144	0.296	1.210	46.6	10.1	-38.21
2	-18.0	1.112	0.406	1.257	48.5	13.6	-42.42
3	-12.0	1.067	0.529	1.185	48.0	18.3	-45.72
4	-6.0	1.107	0.596	1.062	43.8	21.2	-45.79
5	0.0	1.266	0.474	1.062	40.0	16.0	-44.74
6	6.0	1.351	0.324	1.216	42.0	10.1	-42.74
7	12.0	1.255	0.266	1.272	45.4	8.5	-42.11
8	18.0	1.011	0.226	1.123	48.0	8.5	-41.13
9	24.0	0.770	0.217	0.885	49.0	10.5	-16.09

ORIGINAL PAGE IS
OF POOR QUALITY

TABLE XIII

NORMALIZED VELOCITY COMPONENTS, YAW ANGLE, PITCH ANGLE, AND STATIC PRESSURE DIFFERENCE ($p-p_\infty$) FROM AZIMUTHAL TRAVERSE, ϕ = 70 DEG. AT r/D = 0.179

K	THETA (DEG.)	U/UIN	V/UIN	W/UIN	BETA	DELTA	P--PREF
1	-24.0	0.034	-0.564	0.940	87.9	-30.9	-15.94
2	-18.0	0.011	-0.501	1.013	89.4	-26.3	-19.90
3	-12.0	-0.028	-0.445	1.004	91.6	-23.9	-20.27
4	-6.0	-0.017	-0.454	0.904	91.1	-26.7	-17.05
5	0.0	-0.022	-0.507	0.785	91.6	-32.9	-12.72
6	6.0	-0.024	-0.566	0.697	92.0	-39.0	-9.51
7	12.0	-0.049	-0.580	0.779	93.6	-36.6	-12.59
8	18.0	-0.042	-0.575	0.849	92.8	-34.1	-15.25
9	24.0	-0.011	-0.538	0.890	90.7	-31.1	-17.20

TABLE XIV

NORMALIZED VELOCITY COMPONENTS, YAW ANGLE, PITCH ANGLE, AND STATIC PRESSURE DIFFERENCE ($p-p_\infty$) FROM AZIMUTHAL TRAVERSE, ϕ = 70 DEG. AT r/D = 0.204

K	THETA (DEG.)	U/UIN	V/UIN	W/UIN	BETA	DELTA	P-PREF
1	-24.0	2.184	0.187	1.866	40.5	3.7	-25.25
2	-18.0	2.087	0.133	1.840	41.4	2.7	-24.29
3	-12.0	1.859	0.174	1.645	41.5	4.0	-22.25
4	-6.0	1.512	0.244	1.343	41.6	6.9	-23.43
5	0.0	1.480	0.337	1.251	40.2	9.9	-23.85
6	6.0	1.883	0.368	1.542	39.3	8.6	-27.46
7	12.0	2.125	0.205	1.783	40.0	4.2	-24.44
8	18.0	2.127	0.126	1.849	41.0	2.6	-23.18
9	24.0	1.909	0.171	1.683	41.4	3.8	-22.15

TABLE XV

NORMALIZED VELOCITY COMPONENTS, YAW ANGLE, PITCH ANGLE, AND STATIC PRESSURE DIFFERENCE ($p-p_\infty$) FROM AZIMUTHAL TRAVERSE, ϕ = 70 DEG. AT r/D = 0.179 MEASURED 0.109 D DOWNSTREAM OF SWIRLER EXIT

K	THETA (DEG.	U/UIN	V/UIN	W/UIN	BETA	DELTA	P-PREF
1	-24.0	0.350	-0.691	1.041	71.4	-32.2	-10.99
2	-18.0	0.503	-0.613	1.246	68.0	-24.5	-16.03
3	-12.0	0.592	-0.523	1.401	67.1	-19.0	-20.74
4	-6.0	0.613	-0.479	1.473	67.4	-16.7	-21.19
5	0.0	0.595	-0.493	1.473	68.0	-17.2	-20.73
6	6.0	0.604	-0.441	1.495	68.0	-15.3	-21.83
7	12.0	0.621	-0.375	1.544	68.1	-12.7	-23.21
8	18.0	0.565	-0.350	1.526	69.7	-12.2	-22.75
9	24.0	0.470	-0.358	1.483	72.4	-13.0	-23.62

TABLE XVI

NORMALIZED VELOCITY COMPONENTS, YAW ANGLE, PITCH ANGLE, AND STATIC PRESSURE DIFFERENCE ($p-p_\infty$) FROM AZIMUTHAL TRAVERSE, ϕ = 70 DEG. AT r/D = 0.204 MEASURED 0.109 D DOWNSTREAM OF SWIRLER EXIT

K	THETA (DEG.)	U/UIN	V/UIN	W/UIN	BETA	DELTA	P-PREF
1	-24.0	2.023	-0.129	2.608	52.2	-2.2	-25.43
2	-18.0	2.155	-0.042	2.798	52.4	-0.7	-27.87
3	-12.0	2.007	-0.055	2.588	52.2	-1.0	-27.34
4	-6.0	1.805	-0.089	2.270	51.5	-1.8	-18.39
5	0.0	1.913	-0.059	2.271	49.9	-1.1	-17.06
6	6.0	2.265	-0.011	2.643	49.4	-0.2	-25.08
7	12.0	2.307	0.046	2.789	50.4	0.7	-26.46
8	18.0	2.105	0.064	2.627	51.3	1.1	-28.21
9	24.0	1.755	-0.021	2.270	52.3	-0.4	-22.52

TABLE XVII

CALIBRATION SENSITIVITY COMPARISON, ACTUAL VS. 10% HIGHER PITCH COEFFICIENT ONLY

		Percent Difference		
K	θ (deg.)	u/u_{in}	v/u_{in}	w/u_{in}
1	-24.0	1.91	-8.22	1.91
2	-18.0	0.80	-10.23	0.80
3	-12.0	0.27	-11.43	0.27
4	-6.0	0.92	-10.01	0.92
5	0.0	2.15	-7.89	2.15
6	6.0	1.87	-7.27	2.87
7	12.0	2.55	-7.51	2.55
8	18.0	2.29	-7.73	2.29
9	24.0	1.93	-8.17	1.93

TABLE XVIII

CALIBRATION SENSITIVITY COMPARISON, ACTUAL VS. 10% HIGHER VELOCITY COEFFICIENT ONLY

		Percent Difference		
K	θ (deg.)	u/u_{in}	v/u_{in}	w/u_{in}
1	-24.0	4.86	4.86	4.86
2	-18.0	4.88	4.88	4.88
3	-12.0	4.88	4.88	4.88
4	-6.0	4.88	4.88	4.88
5	0.0	4.86	4.86	4.86
6	6.0	4.88	4.88	4.88
7	12.0	4.87	4.87	4.87
8	18.0	4.87	4.87	4.87
9	24.0	4.86	4.86	4.86

TABLE XIX

CALIBRATION SENSITIVITY COMPARISON, ACTUAL VS. 10% HIGHER, BOTH PITCH AND VELOCITY COEFFICIENTS

		Percent Difference		
K	θ (deg.)	u/u_{in}	v/u_{in}	w/u_{in}
1	-24.0	6.87	-3.75	6.87
2	-18.0	5.72	-5.85	5.72
3	-12.0	5.15	-7.12	5.15
4	-6.0	5.84	-5.62	5.84
5	0.0	7.12	-3.41	7.12
6	6.0	7.88	-2.75	7.88
7	12.0	7.54	-3.01	7.54
8	18.0	7.27	-3.25	7.27
9	24.0	6.90	-3.70	6.90

TABLE XX

SWIRL NUMBERS S AND S' FROM RADIAL TRAVERSES

ϕ	S	S'	w_{mo}/u_{mo}
38	0.567	0.559	0.801
45	0.765	0.718	0.876
60	0.850	0.759	0.937
70	0.883	0.750	0.887

TABLE XXI

THEORETICAL SWIRL NUMBERS
BY TWO METHODS

ϕ	Ideal Case I		Most Appropriate Case		
	S	S'	Case	S	S'
38	0.750	0.521	I	0.786	0.534
45	1.333	0.667	III	1.137	0.584
60	-2.309	1.155	V	1.291	0.625
70	-0.660	1.832	V	1.066	0.591

APPENDIX B

FIGURES

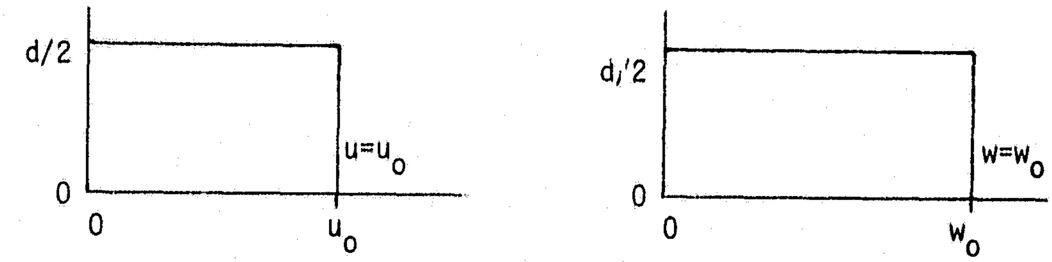

(a) Case I - Flat Axial and Swirl Profiles

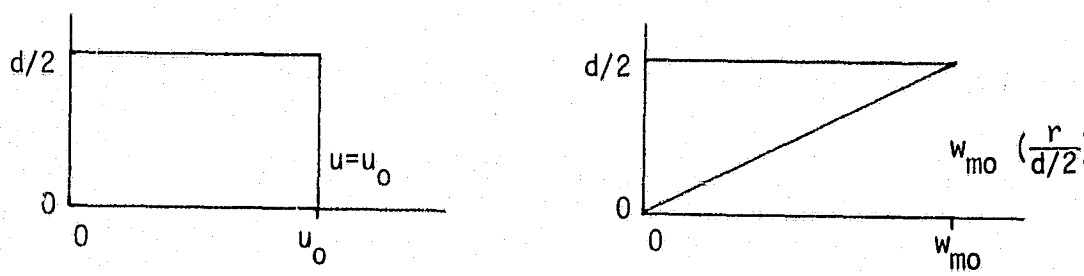

(b) Case II - Flat Axial and Linear Swirl Profiles

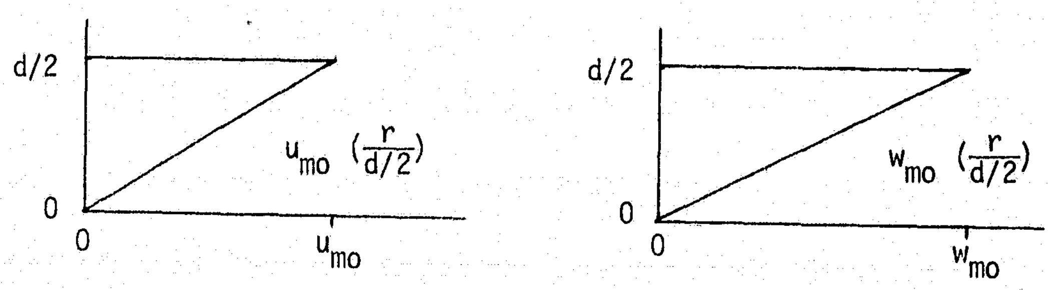

(c) Case III - Linear Axial and Swirl Profiles

Figure 1. Idealized Axial and Tangential Velocity Profile Cases

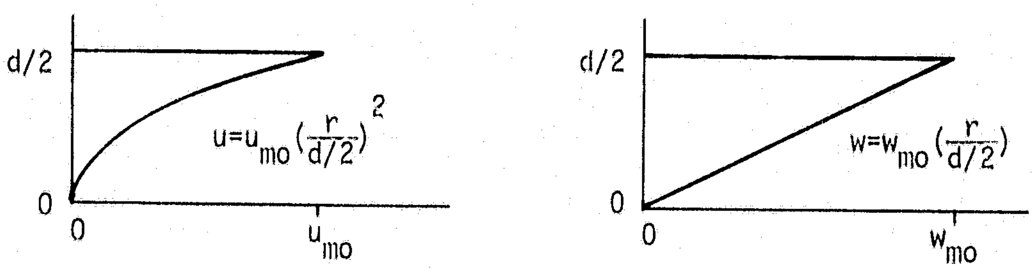

(d) Case IV - Parabolic Axial and Linear Swirl Profiles

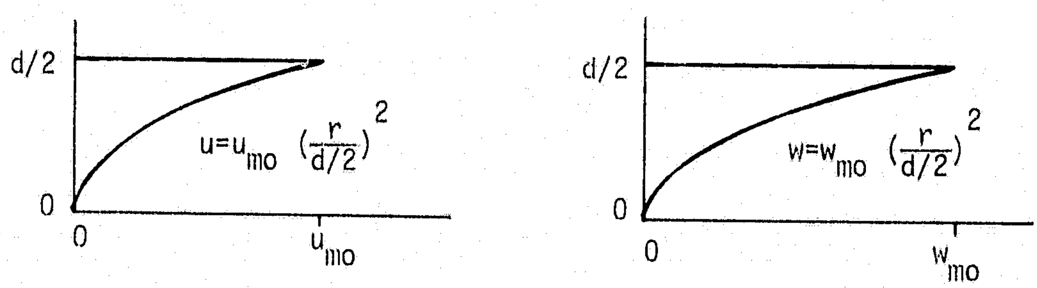

(e) Case V - Parabolic Axial and Swirl Profiles

Figure 1 (continued)

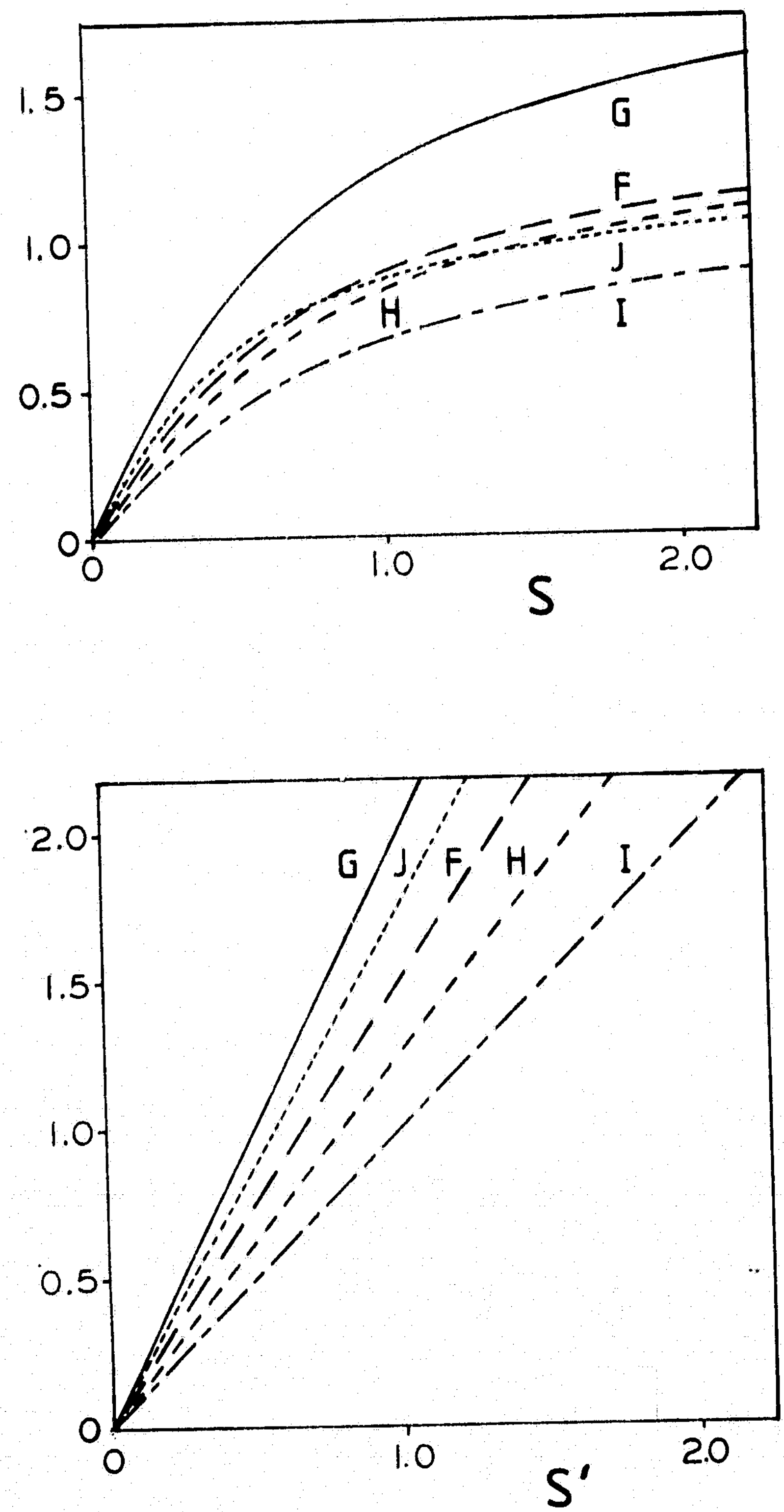

Figure 2. Variation of Velocity Ratios F Through J (Cases I Through V, respectively) with S and S'

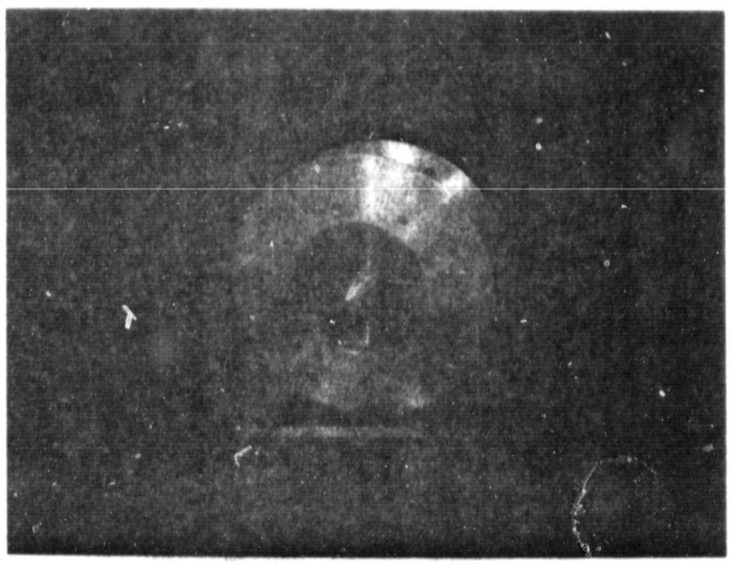

Figure 3. Photograph of Swirler - Upstream End

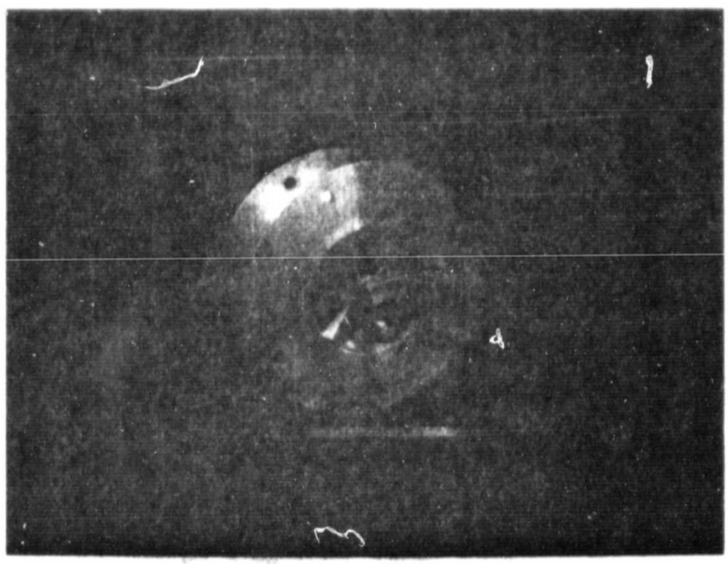

Figu e 4. Photograph of Swirler - Downstream End

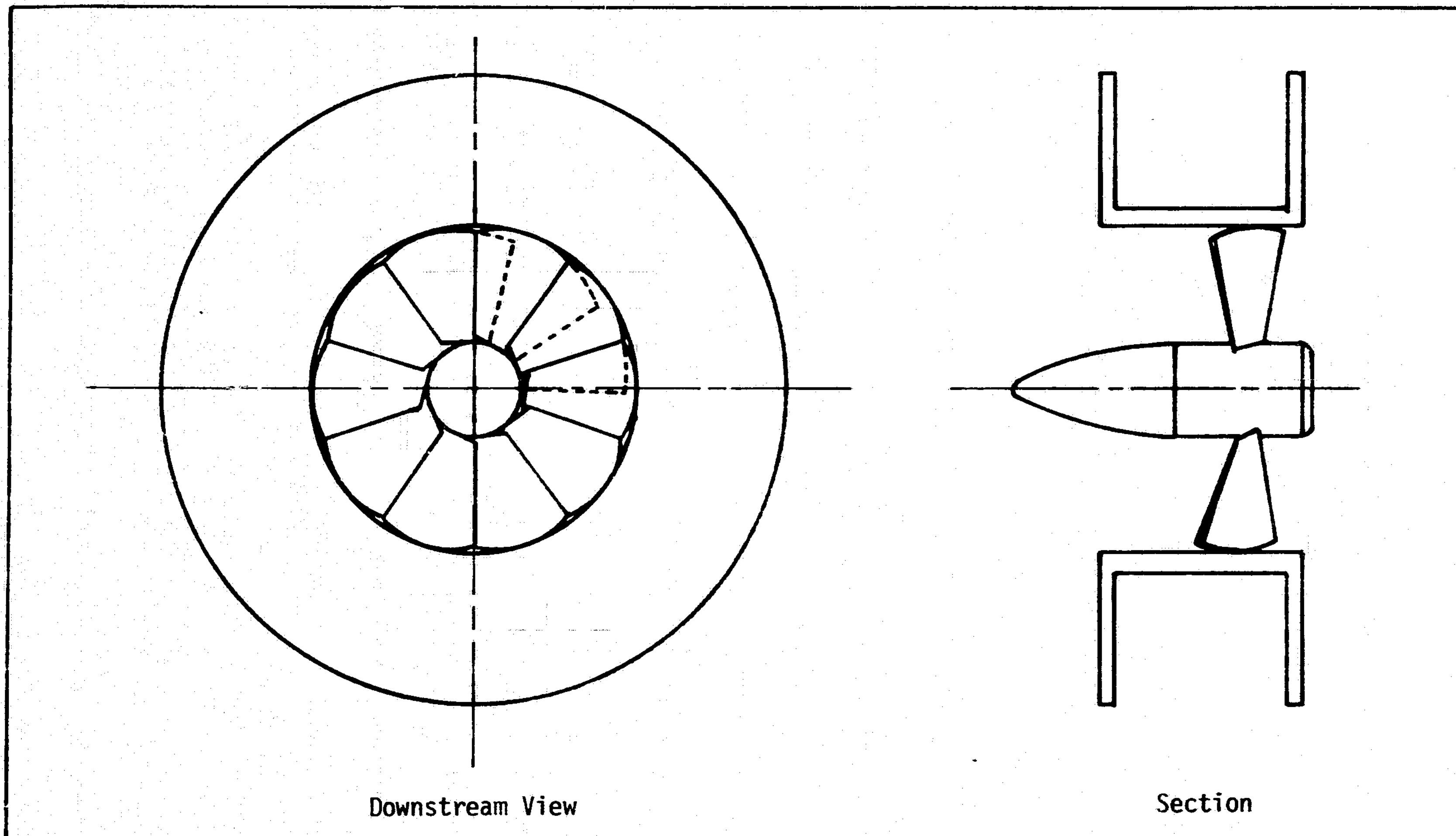

Figure 5. Diagram of Swirler - Section and Downstream View

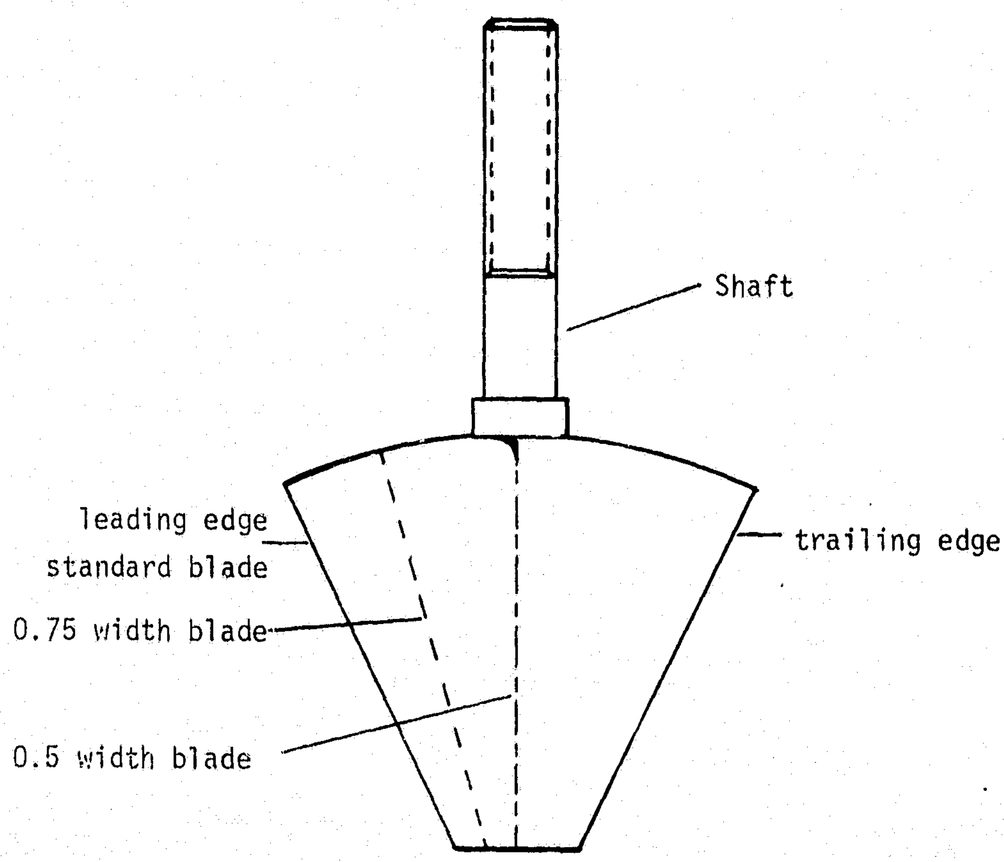

Figure 6. Swirl Vanes

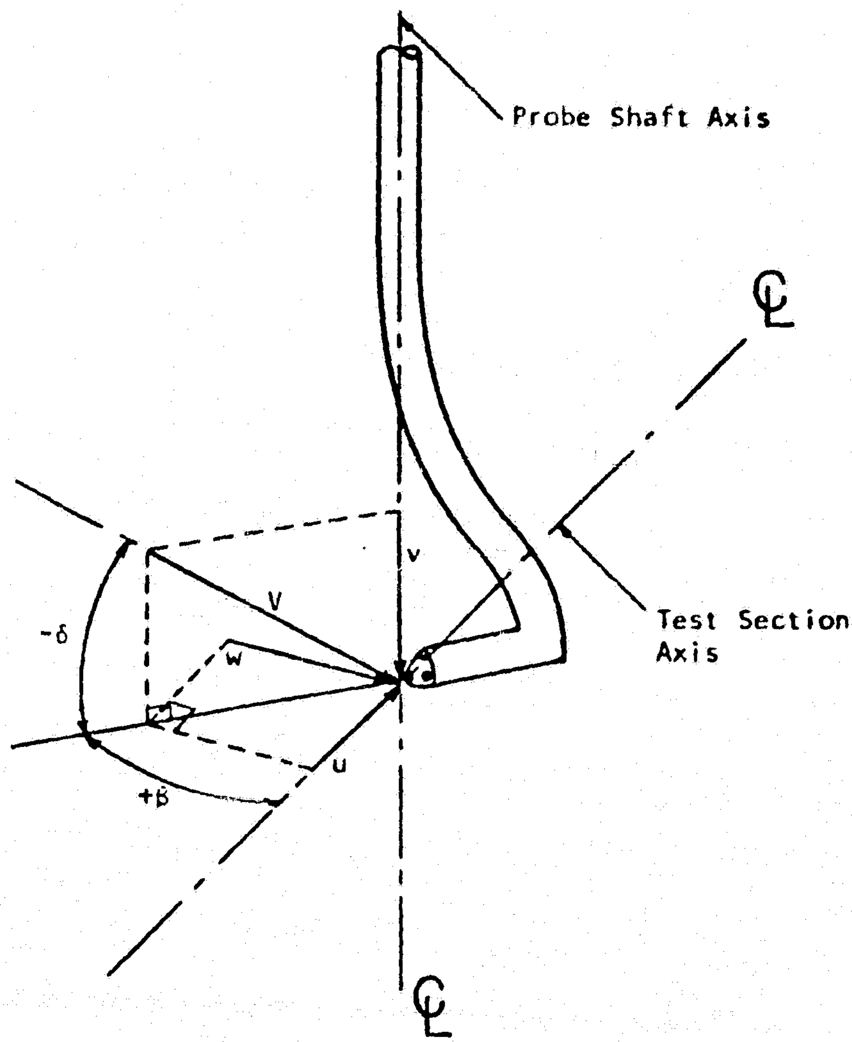

Figure 7. Five-Hole Pitot Probe With Angles and Velocities Measured

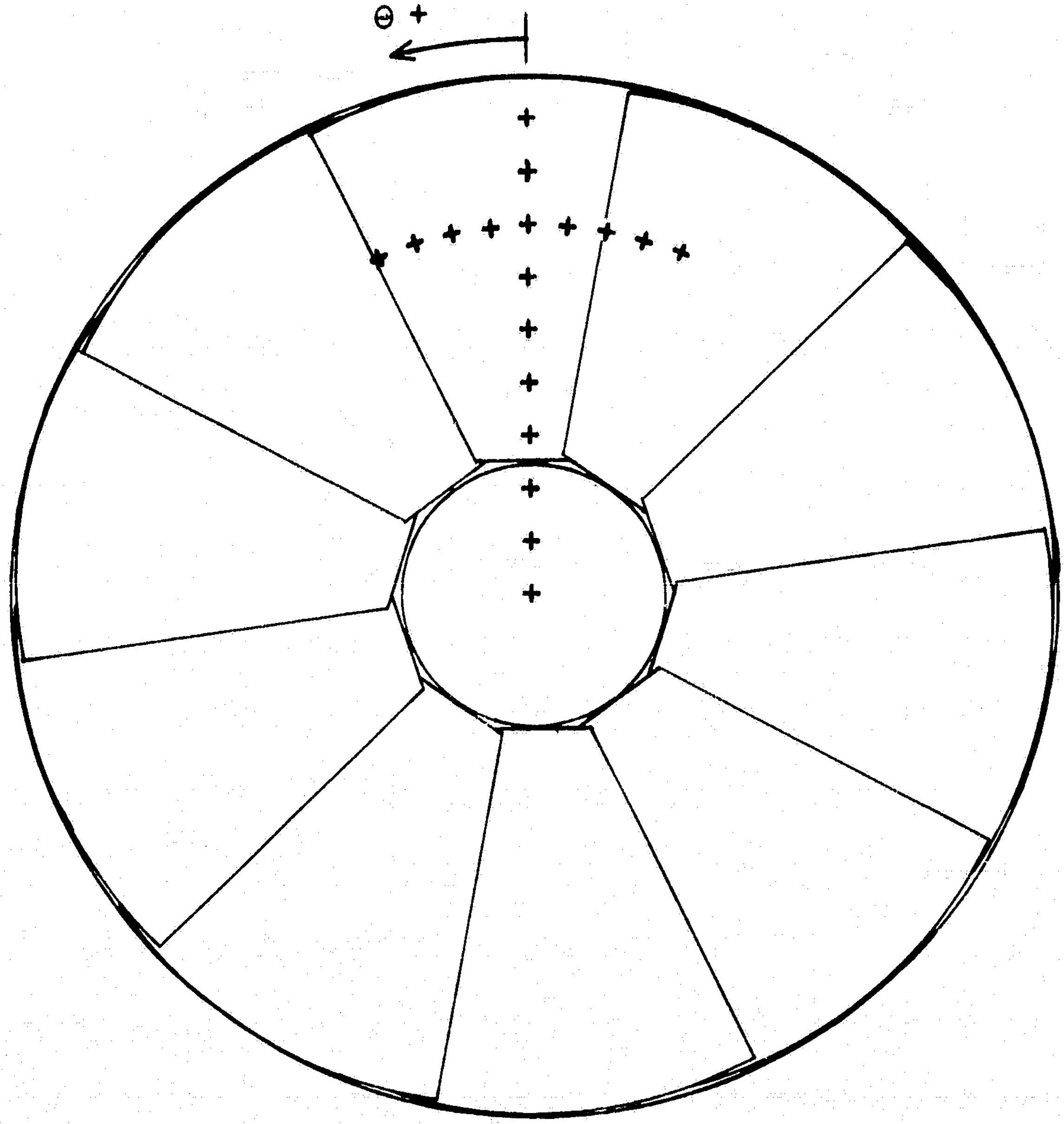

Figure 8. Measurement Locations - Radial and Azimuthal Traverses

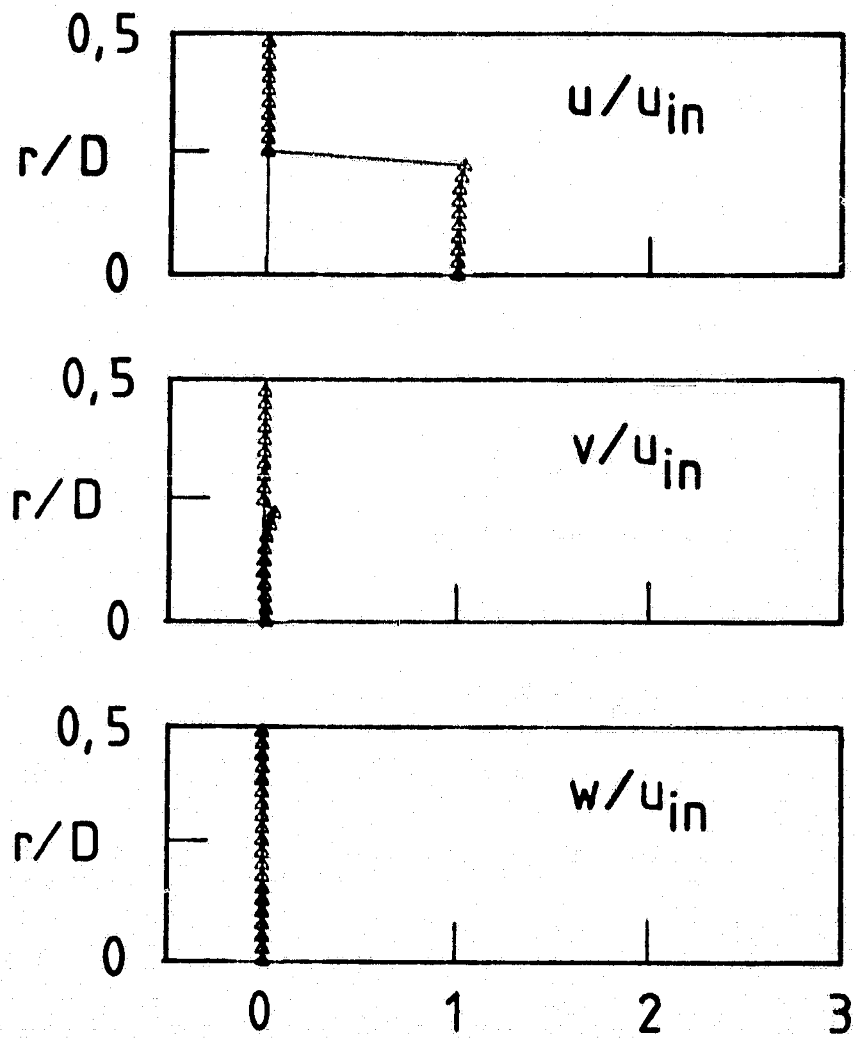

Figure 9. Normalized Velocity Profiles From Radial Traverse, ϕ = 0 deg. (No Swirler)

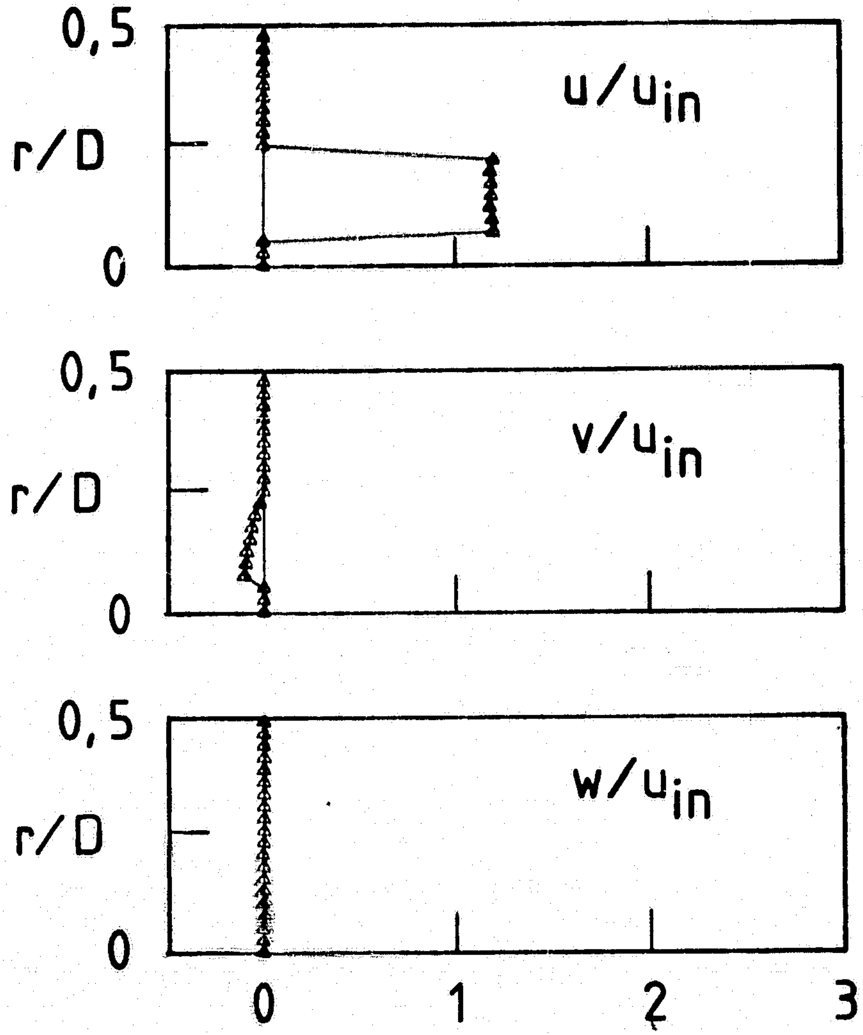

Figure 10. Normalized Velocity Profiles From Radial Traverse, ϕ = 0 deg. (Swirler Installed)

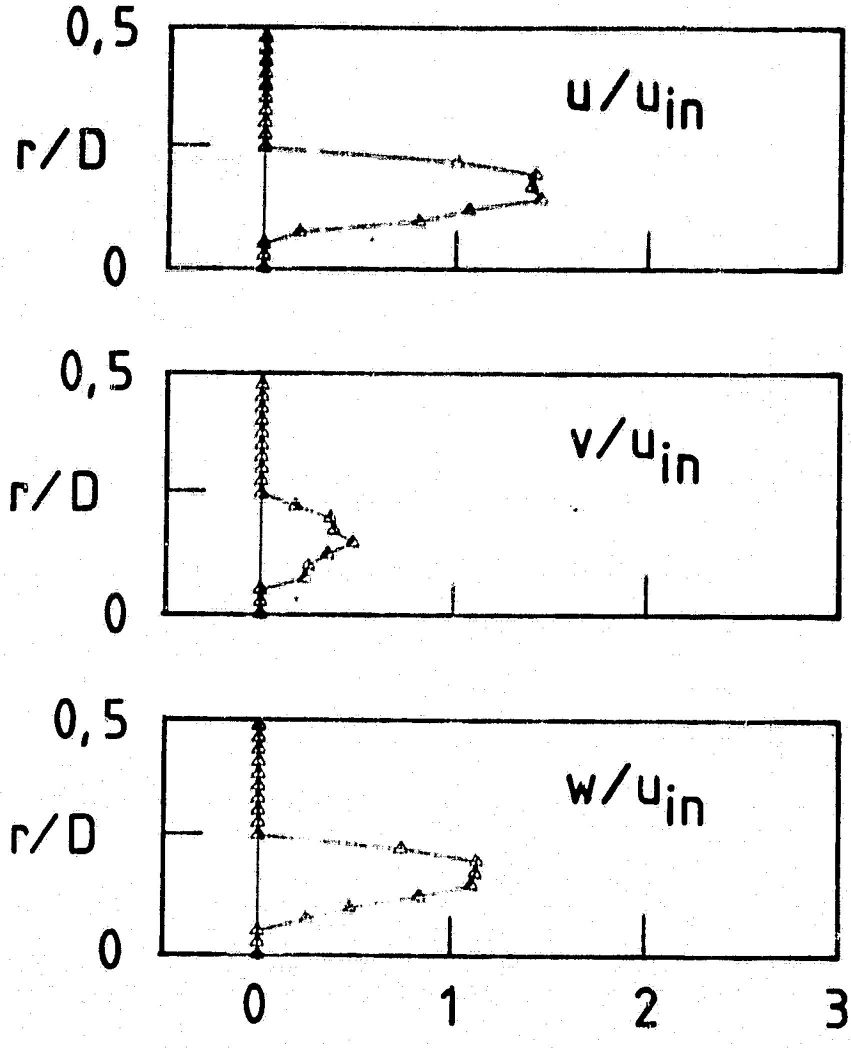

Figure 11. Normalized Velocity Profiles From Radial Traverse, ϕ = 38 deg.

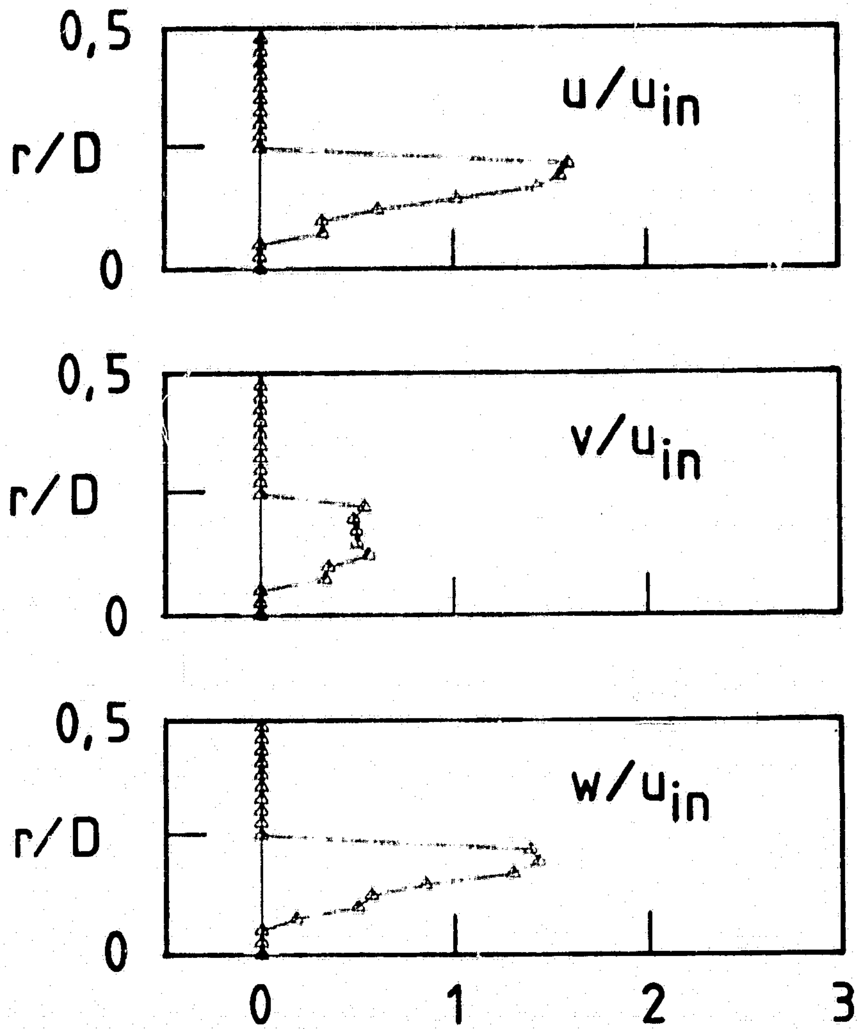

Figure 12. Normalized Velocity Profiles From Radial Traverse, ϕ = 45 deg.

ORIGINAL PAGE IS
OF POOR QUALITY

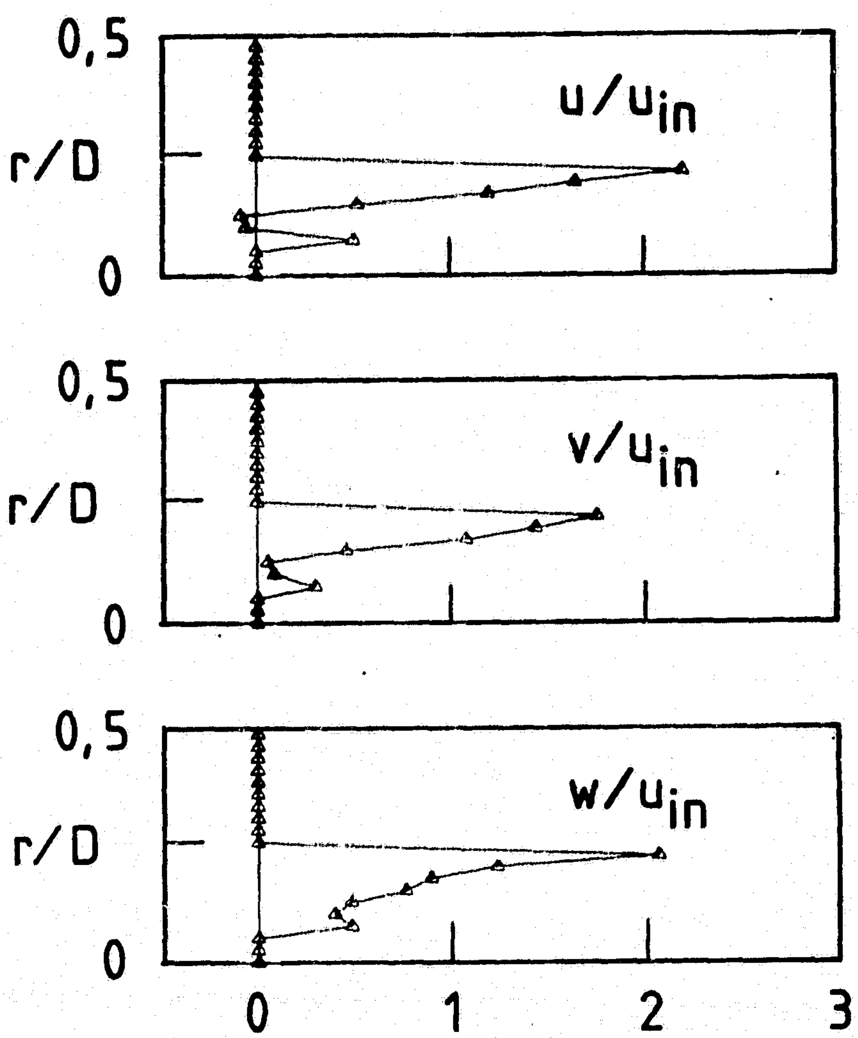

Figure 13. Normalized Velocity Profiles From Radial Traverse, ϕ = 60 deg.

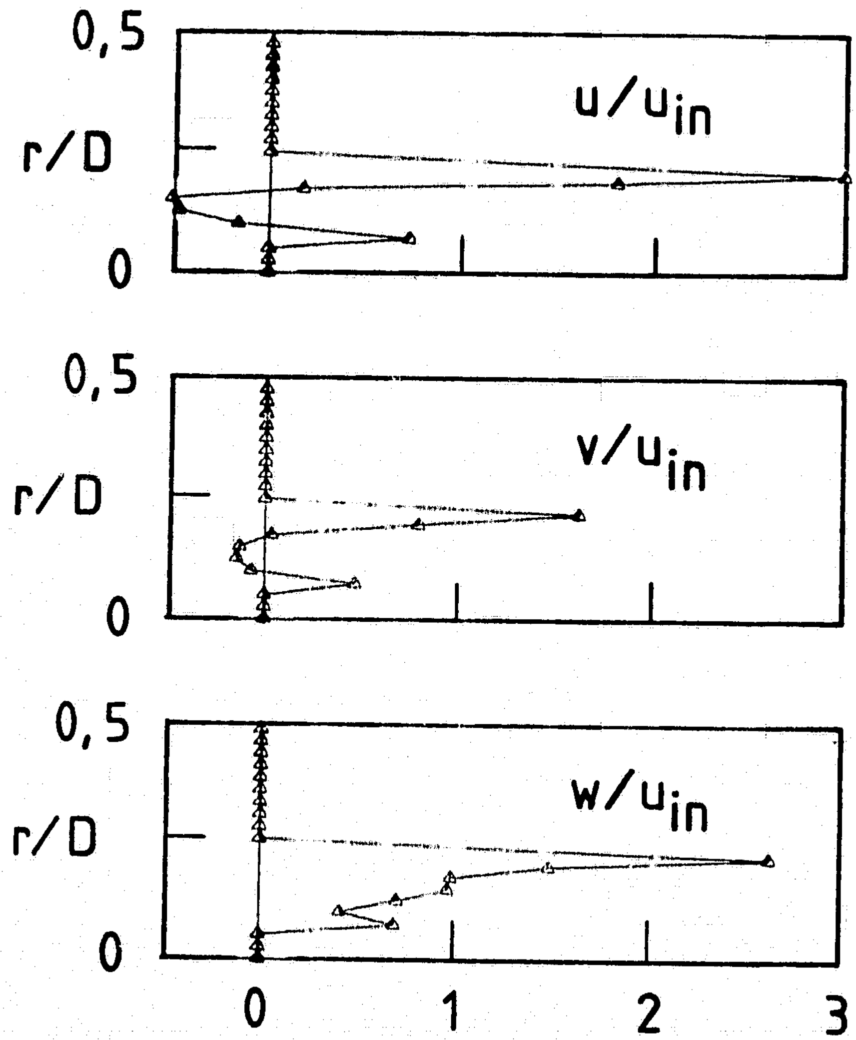

Figure 14. Normalized Velocity Profiles From Radial Traverse, ϕ = 70 deg.

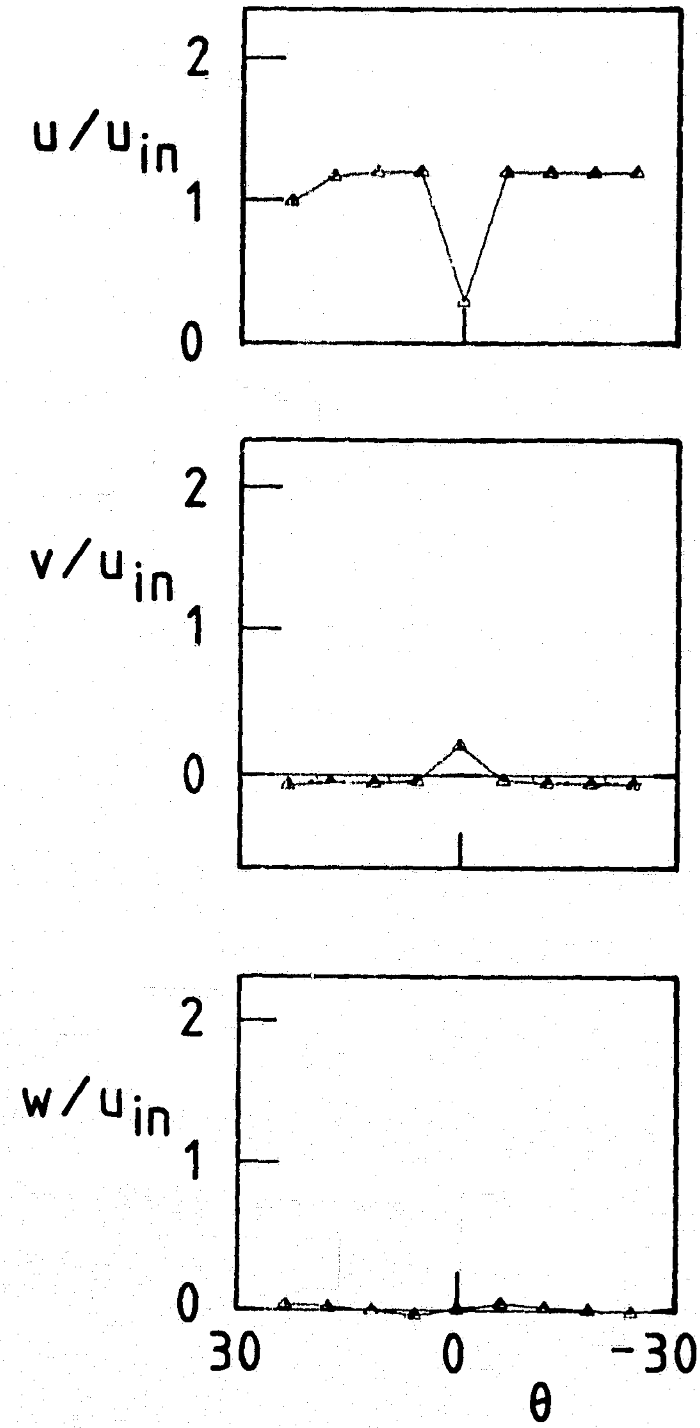

Figure 15. Normalized Velocity Profiles From Azimuthal Traverse, ϕ = 0 deg. at r/D = 0.179 (Swirler Installed)

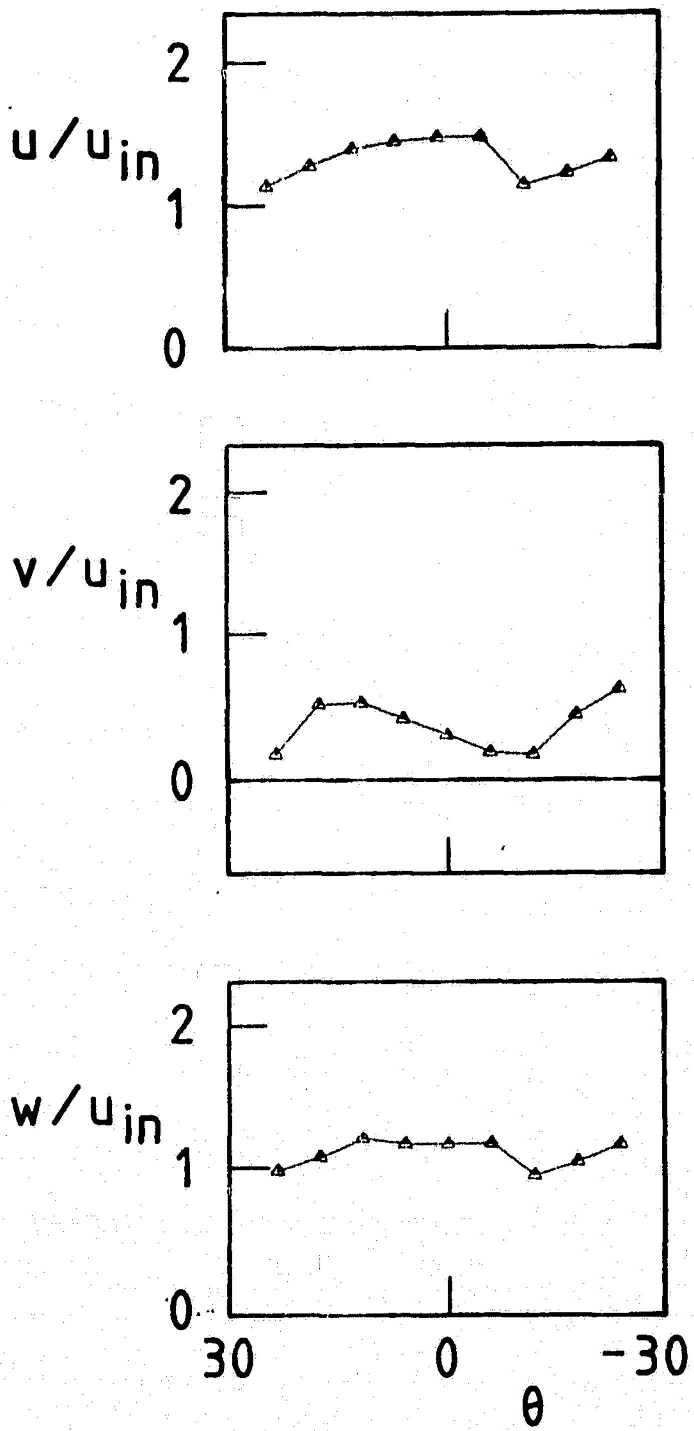

Figure 16. Normalized Velocity Profiles From Azimuthal Traverse, ϕ = 38 deg. at r/D = 0.179

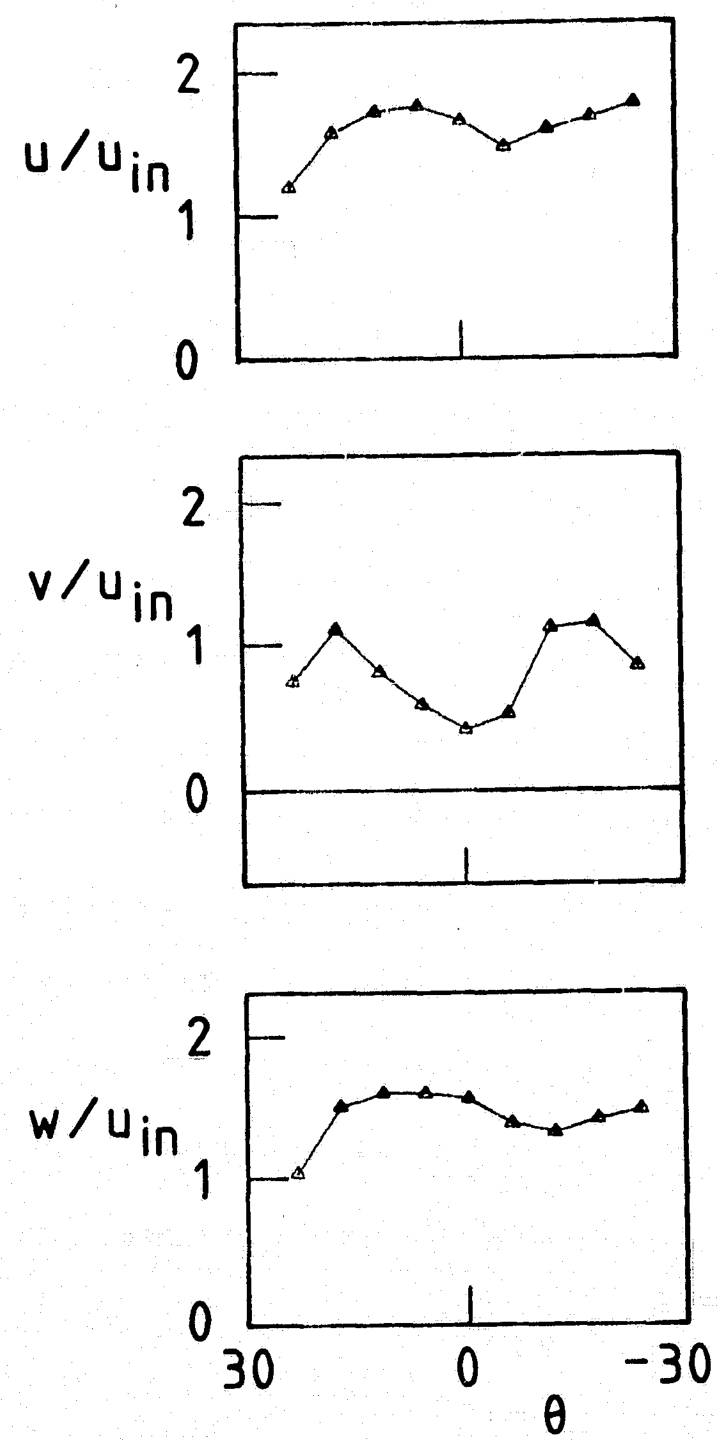

Figure 17. Normalized Velocity Profiles From Azimuthal Traverse, ϕ = 45 deg. at r/D = 0.179

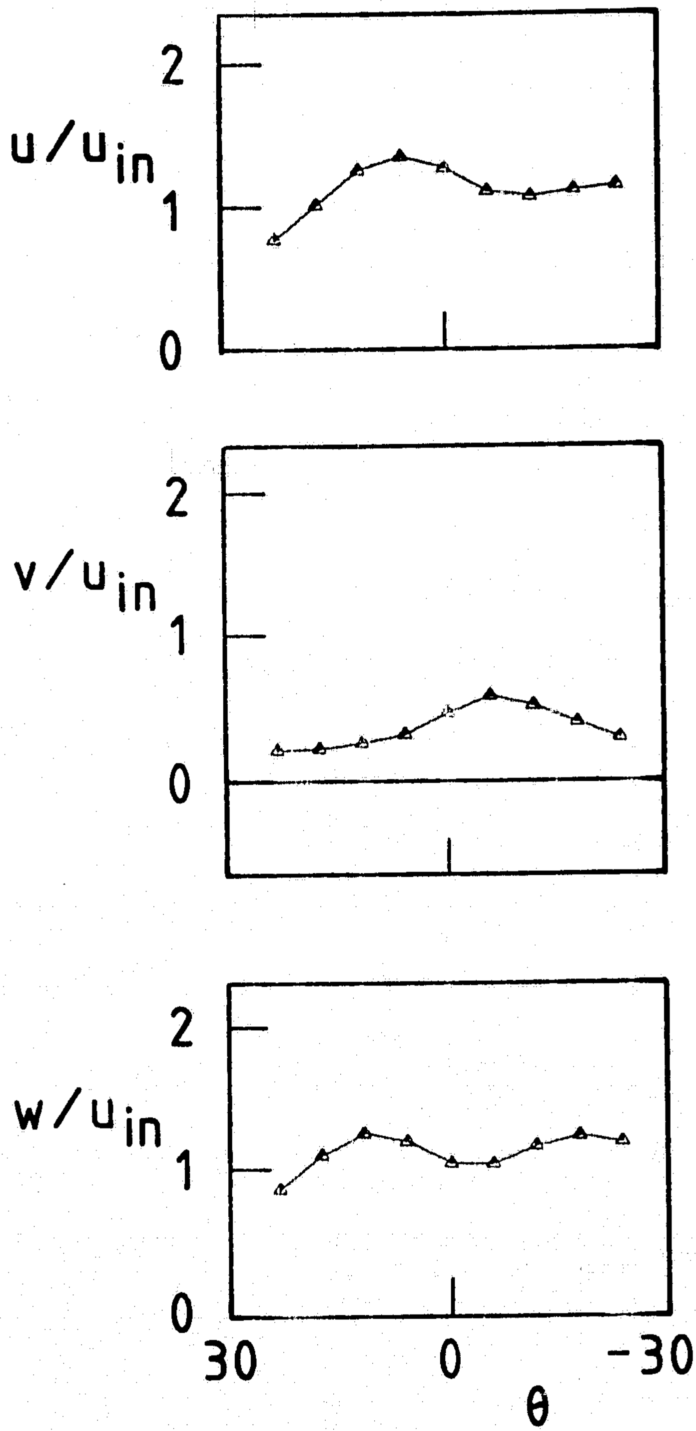

Figure 18. Normalized Velocity Profiles From Azimuthal Traverse, ϕ = 60 deg. at r/D = 0.179

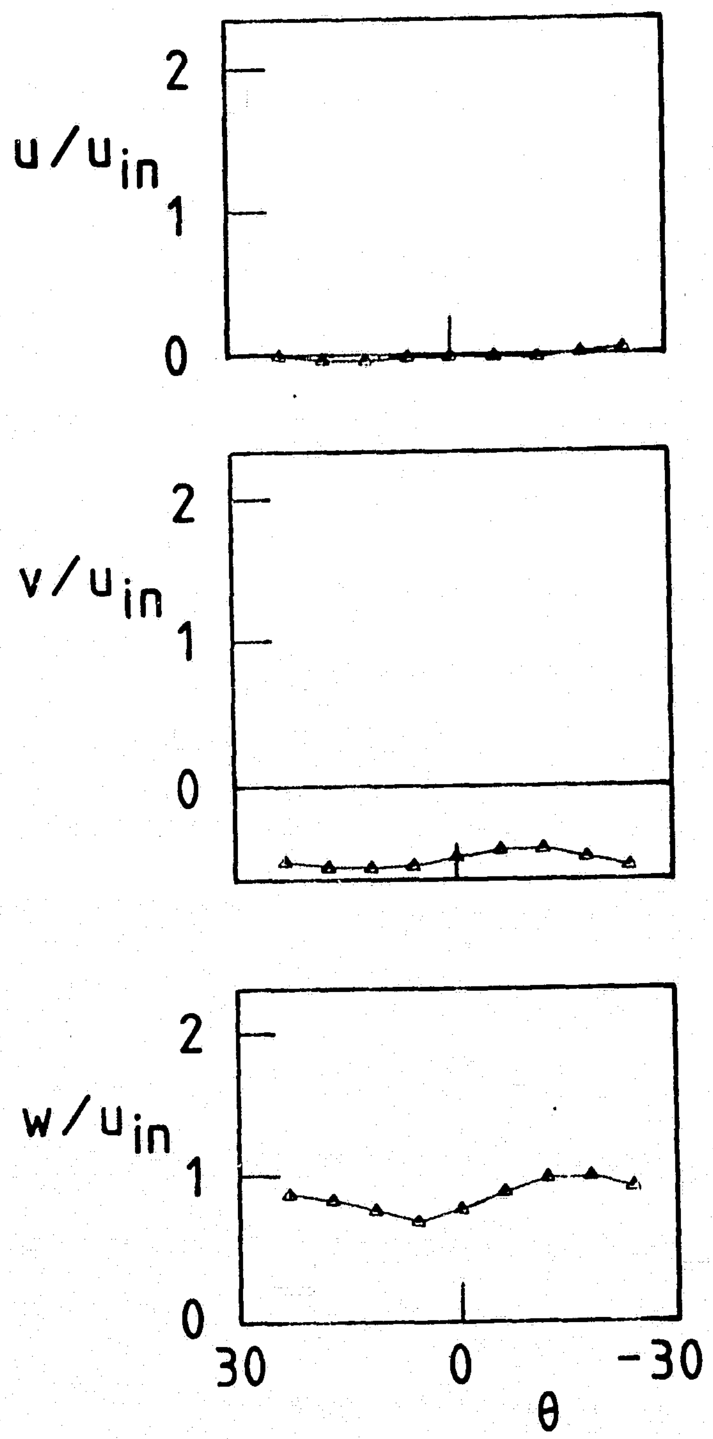

Figure 19. Normalized Velocity Profiles From Azimuthal Traverse, ϕ = 70 deg. at r/D = 0.179

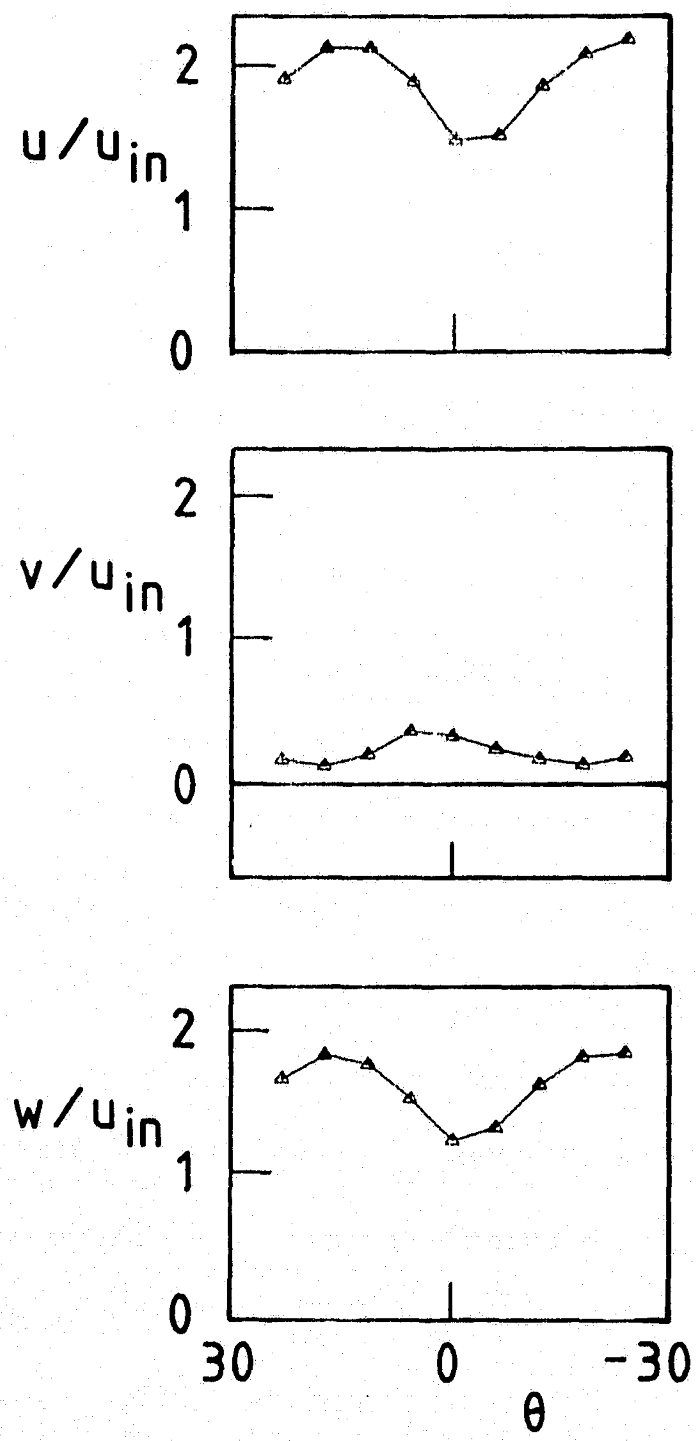

Figure 20. Normalized Velocity Profiles From Azimuthal Traverse, ϕ = 70 deg. at r/D = 0.204

ORIGINAL PAGE IS
OF POOR QUALITY

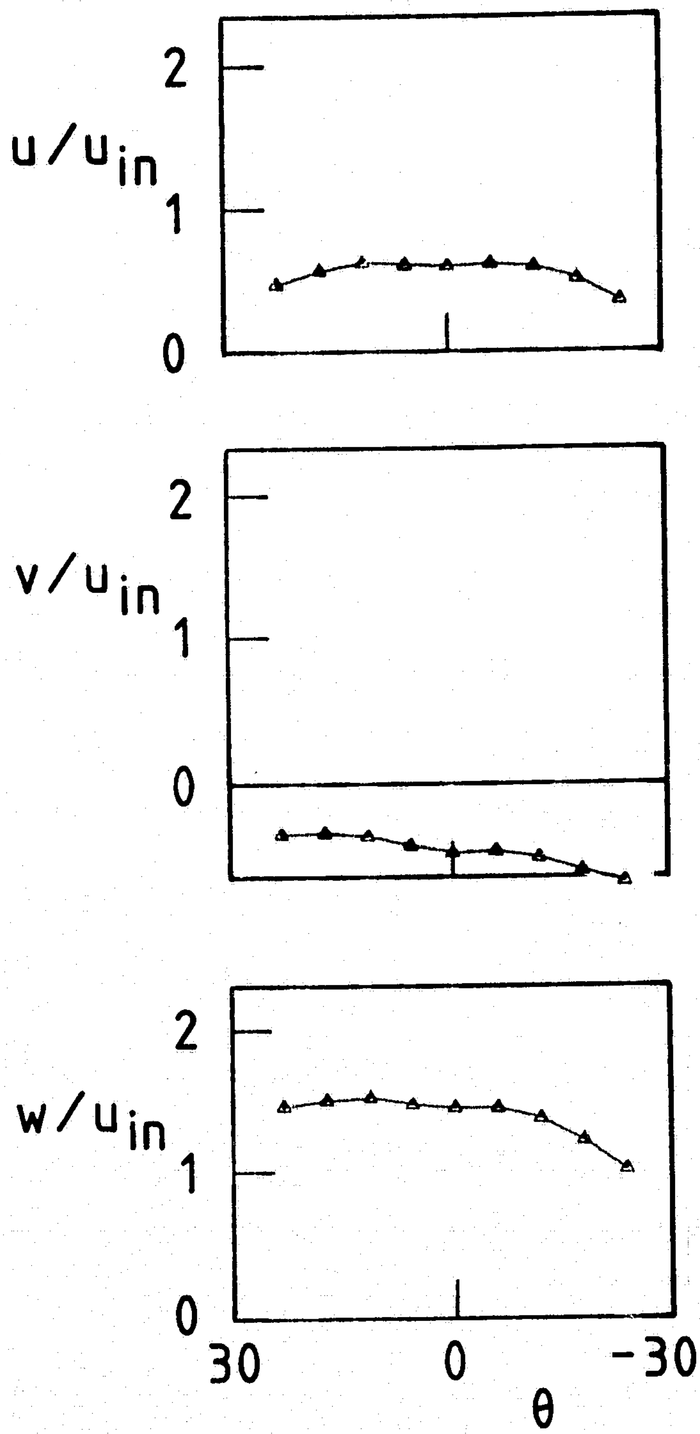

Figure 21. Normalized Velocity Profiles From Azimuthal Traverse, ϕ = 70 deg. at r/D = 0.179 Measured 0.109 D Downstream of Swirler Exit

ORIGINAL PAGE IS
OF POOR QUALITY

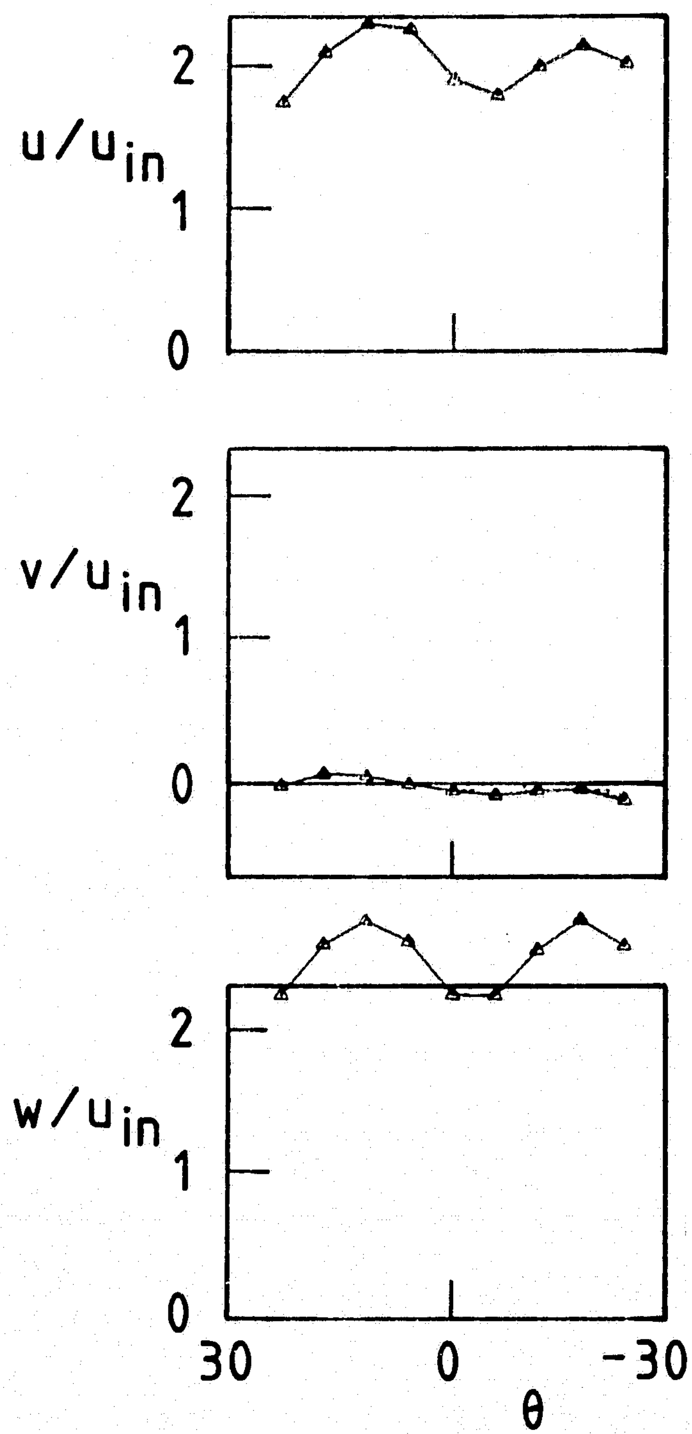

Figure 22. Normalized Velocity Profiles From Azimuthal Traverse, ϕ = 70 deg. at r/D = 0.204 Measured 0.109 D Downstream of Swirler Exit

APPENDIX C

DESCRIPTION OF REVISIONS TO COMPUTER PROGRAM

FOR FIVE-HOLE PITOT DATE REDUCTION

APPENDIX C

The data reduction program used for this project is a modification of a program written by Rhode (19) and described in some detail by Yoon (20). A brief overview of the entire program will be given, followed by a more detailed description of the major changes.

1. Program Overview

The reduction program consists of a main program, two function subprograms, and five subroutines. The main program first calls subroutine INIT to initialize all array variables to zero, then reads in calibration data, control parameters, and the data to be reduced. The actual data reduction is done by repeated calls to the function SPLINE, which uses a cubic spline interpolation method to find pitch angle, velocity, and static pressure at each point from the calibration data. The function H and subroutines ABUILD and GAUSS are called from SPLINE as part of this process.

Next a set of auxiliary calculations are performed. These include nondimensionalizing the output values, calculating momentum fluxes and swirl numbers for radial traverses, and computing averages of the output quantities over successive one-blade cycles for azimuthal traverses. Finally, the primary output values are written into an unformatted output data set for disk storage, and all output variables are printed out in standard format using the subroutines WRITE and PRINT.

Changes were made to two sections of Rhode's original program: the main program and subroutine INIT. For brevity, only the changes to these sections will be considered in detail here. For information on the structure and function of the unmodified parts of the program, see Reference 20.

2. Additions and Modifications

The code's new capabilities include calculation of static pressure at each location and reduction of either radial or azimuthal traverse data. For radial traverses, the code calculates axial flux of axial momentum (with and without static pressure contribution) and swirl numbers S and S'. For azimuthal traverses, it calculates averages of the output values u, v, w, and $p - p_\infty$. In addition, substantial changes have been made in the way data is labeled, read in, and stored, in an effort to reduce storage requirements and make the code easier to use and understand.

Static Pressure Calculation

The static pressure is found using a method based on one described by Bryer and Pankhurst (21). The method uses the fact that the absolute pressure at any of the five holes in the probe tip can be expressed as

$$p_i = p_{st} + K_i q$$

where p_{st} is the local static pressure, K is an empirical coefficient which is a function of pitch angle δ, q is the local dynamic pressure

$\frac{1}{2}\rho \bar{V}^2$, and the subscript i stands for any of the ports N, S, E, W, or C. Rearranging this and subtracting atmospheric pressure from both sides, we obtain for the central pressure port

$$p_{st} - p_{atm} = (p_C - p_{atm}) - K_C q \tag{C.1}$$

We now introduce the velocity coefficient,

$$VC = \frac{\frac{1}{2}\rho \bar{V}^2}{(p_C - p_W)} = \frac{q}{(p_C - p_W)}$$

which is already used in the code to determine total velocity magnitude. In accordance with standard practice, it is assumed that the velocity coefficients under calibration and measurement conditions are identical at a given pitch angle δ_1, regardless of differences in fluid velocity. That is, $VC_{\delta_1,cal} = VC_{\delta_1,meas}$ or

$$\frac{q_{cal}}{(p_C - p_W)_{\delta_1,cal}} = \frac{q_{meas}}{(p_C - p_W)_{\delta_1,meas}}$$

This rearranges to

$$q_{meas} = \frac{q_{cal}}{(p_C - p_W)_{\delta_1,cal}} \cdot (p_C - p_W)_{\delta_1,meas} \tag{C.2}$$

Now, from Equation (C.1), taken at δ_1 under calibration conditions:

$$K_{C_{\delta_1,cal}} = \left[\frac{p_C - p_{st}}{q}\right]_{\delta_1,cal} = \frac{(p_C - p_{atm})_{\delta_1,cal}}{q_{cal}},$$

since the static pressure equals atmospheric pressure in the free jet used for calibration. Substituting this and Equation (C.2) into

Equation (C.1), we get

$$(p_{st} - p_{atm})_{meas} = (p_C - p_{atm})_{\delta_1,meas} -$$

$$\left[\frac{(p_C - p_{atm})_{\delta_1,cal}}{q_{cal}}\right]\cdot\left[\frac{q_{cal}}{(p_C - p_W)_{\delta_1,cal}}\ (p_C - p_W)_{\delta_1,meas}\right]$$

The calibration dynamic pressure cancels, and the remaining calibration pressures may be combined to form a dimensionless static pressure coefficient,

$$SPC = \frac{(p_C - p_{atm})}{(p_C - p_W)}$$

which is determined as a function of δ from calibration data. This leads to the final expression for the gage static pressure at a location where the pitch angle is δ_1:

$$(p_{st} - p_{atm})_{\delta_1,meas} = (p_C - p_{atm})_{\delta_1,meas} - SPC_{\delta_1}\ (p_C - p_W)_{\delta_1,meas}$$

This last expression is used directly in the code. The value of SPC is found by the same third-order spline interpolation technique used to find the pitch and velocity coefficients at each measurement location. (See lines 2690-2720 and line 3070 in the listing in Appendix D.)

Radial and Azimuthal Capability

The reduction of both radial and azimuthal traverses was implemented by the addition of an integer flag in the input data to indicate which type of traverse is to be reduced. This flag, the variable KRADTR, is given a value of 1 for radial traverses and 0 for azimuthal ones. Since this value is read in only once for the entire run, all traverses to be reduced in a single run must be of the same type - either all radial or all azimuthal.

Data for both traverse types is treated identically through Chapter I of the code, with the azimuth angles read in as values of radius, RINCHS. The major differences occur in Chapter II where the auxiliary calculations are performed. Depending on the value of KRADTR, radius values are nondimensionalized by the test section diameter or reset so that azimuth values remain in degrees. Next, the value of KRADTR is used to control branching to program segments which perform calculations unique to each traverse type, which are described in the next two sections. The last application of KRADTR is in Chapter III, Output. Here again, it controls branching to ensure that only those output values appropriate to the traverse type being reduced are printed out.

Radial Traverse Calculations

When reducing data from radial traverses, the code automatically performs a simple numerical integration procedure to find approximate values of mass flow rate and the momentum fluxes G_Θ, G_x, and G_x'. These values are then used to calculate the swirl numbers S and S' as defined in Chapter II.

The integration procedure is effectively the same as that used by Rhode in his original reduction code, as well as in the STARPIC prediction code (22). However, the integration has been rewritten to calculate terms for the ring elements in a more straight-forward manner, and the central disk element has been added for completeness (lines 3830 through 3880 of Appendix D).

In the absence of true static pressure taps in the rim of the swirler, the reference pressure p_∞ has been approximated by the measured static pressure at the measurement location nearest the wall of the swirler. This may introduce an error, but the results will still be useful for comparing trends.

Azimuthal Traverse Calculations

For the azimuthal data, an averaging procedure is used instead of the integration routine. Since the data is expected to be cyclic with a period of one blade width, averaging is performed over successive one-blade cycles. These successive averages may then be compared to check deviation from cyclic behavior or averaged again to get a single representative value for each of the major output quantities.

The code is set up to handle traverses having six points over the width of one blade; for example, six-degree increments for a ten-bladed swirler. For other spacings the value of NREP (line 4470 of the code) must be changed.

Since the reference pressure p_∞ for each vane angle setting is taken from a radial traverse at the exit plane, the value of p_∞ must be supplied by the user for azimuthal runs. This allows calculation of the pressure difference $p - p_\infty$ from azimuthal traverses for comparison with the values obtained from radial traverses. For those users not concerned with static pressure measurements, the supplied reference pressure PREF may be omitted or set equal to atmospheric pressure.

Miscellaneous Modifications

To make the code easier to use, all primary user inputs have been separated from the body of the code and incorporated into the block of input data, which is stored in a separate dataset. This minimizes the need to make changes in the body of the code, and reduces the memory space required to keep a record of all input data for each run. New headings were added to the input dataset to identify both the calibration and measurement data, and additional variables are stored on disk for use by auxiliary programs which produce tables and profile plots. To improve readability of the code, all DO loops were indented and extensive comments were added. A listing of the reduction code with sample input and output appears in Appendix D.

APPENDIX D

LISTING OF FIVE-HOLE PITOT DATA REDUCTION PROGRAM WITH SAMPLE INPUT DATA

```
C
C***********************************************************************
C
C
C     A COMPUTER PROGRAM FOR DATA REDUCTION OF FIVE-HOLE PITOT
C     MEASUREMENTS IN TURBULENT, SWIRLING, RECIRCULATING FLOW
C     IN COMBUSTOR GEOMETRIES
C
C     VERSION OF MARCH, 1983 --
C     MODIFICATIONS INCLUDE COMBINED RADIAL AND AZIMUTHAL CAPA-
C     BILITY, REDUCTION OF STATIC PRESSURE DATA, AND CALCULATION
C     OF MOMENTUM FLUXES AND SWIRL NUMBERS FOR RADIAL PROFILES.
C
C     BASED ON A PROGRAM BY D. L. RHODE (PHD THESIS, OSU, 1981)
C
C
C     G. F. SANDER
C     MECHANICAL AND AEROSPACE ENGINEERING
C     OKLAHOMA STATE UNIVERSITY
C     STILLWATER, OK     74078
C
C
C***********************************************************************
C
C---MAJOR FORTRAN VARIABLES IN MAIN PROGRAM (LISTED IN ORDER
C             OF FIRST OCCURRENCE IN THE PROGRAM):
C
C IWRITE - LOGICAL FLAG FOR WRITING INTO OUTPUT DATASET (UNFORMATTED)
C DIAGNS - FLAG FOR DIAGNOSTIC OUTPUT
C IT     - MAX NO. OF TRAVERSES ALLOWED; DIMENSION VALUE IN SUBROUTINES
C JT     - MAX NO. OF POINTS ALLOWED PER TRAVERSE; ALSO DIMENSION VALUE
C HEDM ETC. - ALL VARIABLES STARTING WITH 'HED' ARE ALPHANUMERIC ARRAYS
C                  FOR OUTPUT HEADINGS
C NCAL   - NO. OF CALIBRATION DATA POINTS
C CPITCH - CALIBRATION PITCH COEFF. -- (PN-PS)/(PC-PW)
C CDELTA - CAL. PITCH ANGLE -- STANDARD RANGE -58 TO +58 DEG.
C CVELCF - CAL. VELOCITY COEFF. -- (CAL. DYN. PRESS.)/(PC-PW)
C CPSTCF - CAL. STATIC PRESSURE COEFF. -- (PC-PA)/(PC-PW)
C HEDID1,HEDID2 - USER HEADINGS TO IDENTIFY THE RUN BEING REDUCED
C ALPHA  - INLET SIDEWALL EXPANSION ANGLE
C PHI    - SWIRL VANE ANGLE SETTING
C DSINCH - INLET NOZZLE OR SWIRLER DIAMETER, DSMALL, IN INCHES
C DLINCH - TEST SECTION DIAMETER, DLARGE, INCHES
C KRADTR - INTEGER FLAG FOR TRAVERSE TYPE -- 1 FOR RADIAL, 0 FOR AZIM.
C NSTATN - NO. OF TRAVERSES TO BE REDUCES
C MAXJPT - MAX NO. OF POINTS IN ANY OF THE TRAVERSES BEING REDUCED
C XINCHS - AXIAL POSITION OF EACH TRAVERSE, INCHES
C NDATA  - NO. OF DATAPOINTS IN EACH TRAVERSE
C RDNPRS - INLET DYNAMIC PRESSURE (UPSTREAM OF SWIRLER), TORR
C PREF   - REF. PRESS. USED TO CALC. PDIFF FOR SWIRL NUMBER, TORR
C FANSPD - FAN SPEED, RPM
C TFLOW  - TEMPERATURE OF AIR IN TEST SECTION, DEG. CELSIUS
C PATM   - ATMOSPHERIC PRESSURE, TORR
C BZOFF  - BETA ZERO-OFFSET FOR YAW ANGLE READINGS
C RINCHS - RADIAL POS. OF DATAPOINT, INCHES (THETA FOR AZIM. TRAVERSES)
```

**ORIGINAL PAGE IS
OF POOR QUALITY**

```
C RBETA    - RAW VALUE OF YAW ANGLE BETA, DEG.
C RENNPS - MEAS. VALUE OF PNORTH - PSOUTH PRESS. DIFF, TORR
C RPCHEW - MEAS. VALUE OF PCENTER - PWEST, TORR
C RPCMPA - MEAS. VALUE OF PCENTER - PATMOSPHERE, TORR
C RSMALL  - INLET NOZZLE OR SWIRLER RADIUS, METERS
C RLARGE  - TEST SECTION RADIUS, METERS
C X       - AXIAL POSITION OF TRAVERSE, METERS
C R       - RADIAL POSITION OF DATAPOINT, METERS
C IDID    - FLAG TO USE ENTRY POINT SP IN SPLINE INTERPOLATION ROUTINE
C PICHCF  - REDUCED PITCH COEFF. FOR EACH DATAPOINT
C DELTA   - REDUCED PITCH ANGLE FOUND BY INTERPOLATION USING PICHCF
C VELCF   - REDUCED VELOCITY COEFF. FROM INTERPOLATION USING DELTA
C PSTCF   - REDUCED STATIC PRESS. COEFF. FROM INTERPOLATION USING DELTA
C RHO     - DENSITY FOR EACH TRAVERSE, FROM IDEAL GAS LAW
C BETA    - REDUCED VALUE FOR PROBE YAW ANGLE, DEG.
C VTOTAL  - TOTAL VELOCITY VECTOR MAGNITUDE, M/S
C U       - AXIAL COMPONENT OF VELOCITY, M/S
C V       - RADIAL COMP. OF VELOCITY, M/S
C W       - TANGENTIAL (SWIRL) VELOCITY, M/S
C P       - REDUCED VALUE OF STATIC PRESSURE, N/SQ. M (GAGE)
C XND     - NONDIMENSIONAL AXIAL POSITION, X/RLARGE
C UIN     - INLET REFERENCE VELOCITY (CALC. FROM RDNPRS), M/S
C MASFLO  - INLET MASS FLOW RATE (ASSUMING UNIFORM AXIAL VELOCITY), KG/S
C VTSTAR  - NONDIM. TOTAL VELOCITY MAGNITUDE, VTOTAL/UIN
C USTAR   - NONDIM. AXIAL VELOCITY, U/UIN
C VSTAR   - NONDIM. RADIAL VELOCITY, V/UIN
C WSTAR   - NONDIM. TANGENTIAL VEL., W/UIN
C PSTAR   - NONDIM. STATIC PRESSURE, P/RDNPRS
C RND     - NONDIM. RADIAL POS., R/RLARGE; ALSO THETA FOR AZIM. TRAVERSES
C DYPS    - 'DELTA-Y, POINT SOUTH' (FOR RADIAL INTEGRATION; FROM STARPIC)
C DYNP    - 'DELTA-Y, NORTH POINT' (SIM. TO DYPS)
C SNS     - 'SMALL NORTH-SOUTH' FROM STARPIC; USED AS DELTA R FOR INTEGR.
C PDIFF   - PRESS. DIFF. P - PREF USED TO CALCULATE SWIRL NUMBER, N/SQ. M
C AREA1   - AREA OF DISC ELEMENT AT CENTER OF INTEGRATION REGION
C FLOW    - SUMMATION FOR MASS FLOW THROUGH RING ELEMENTS
C WMOM    - SUMMATION FOR ANGULAR MOMENTUM FLUX
C UMOM    - SUMMATION FOR DYNAMIC AXIAL MOM. FLUX (NEGL. PRESS. TERM)
C UMOMP   - SUMMATION FOR AXIAL MOMENTUM FLUX, INCL. PRESSURE DIFF. TERM
C AREAJ   - AREA OF EACH RING ELEMENT, SQ. M
C MASS    - INTEGRATED MASS FLOW RATE, KG/S
C UMEAN   - INTEGRATED MEAN AXIAL VELOCITY, M/S
C ANGMOM  - INTEGRATED AXIAL FLUX OF ANGULAR MOMENTUM, N-M
C AXMOM   - INT. AXIAL FLUX OF DYNAMIC AXIAL MOM., N (NEGL. PRESS. TERM)
C AXMOMP  - INT. AXIAL FLUX OF AXIAL MOMENTUM, N (INCL. PRESSURE TERM)
C SPRIME  - SWIRL NUMBER CALC. USING DYNAMIC AXIAL MOMENTUM FLUX
C S       - SWIRL NUMBER CALC. USING FULL AXIAL MOM. FLUX (INCL. PRESS.)
C USTAVG  - AVERAGE OF USTAR VALUES FOR AZIM. TRAV., OVER ONE BLADE SPACE
C VSTAVG  - AVG. OF VSTAR VALUES
C WSTAVG  - AVG. OF WSTAR VALUES
C PDFAVG  - AVG. OF PDIFF VALUES
C VISCOS  - LAMINAR ABS. VISCOSITY CALCULATED FOR EACH TRAVERSE, KG/M*S
C REDIN   - INLET REYNOLDS NUMBER, CALC. USING VISCOSITY FOR EACH TRAV.
C
C
CHAPTER  0  0  0  0  0  0  0  0  PRELIMINARIES  0  0  0  0  0  0  0  0
C
      DIMENSION HEDM(9),HEDUMN(9),HEDNMS(9),HEDCMW(9),HEDCMA(9),
     #HEDU(9),HEDV(9),HEDW(9),HEDVT(9),HEDUST(9),
     #HEDVST(9),HEDWST(9),HEDPST(9),HEDDEL(9),HEDBET(9),
     #HEDMMF(9),HEDMIV(9),HEDMIP(9),HEDAM(9),
     #HEDAX(9),HEDAXP(9),HEDSPR(9),HEDS(9),HEDP(9),HEDPDF(9),HEDRED(9),
     #HEDID1(18),HEDID2(18),HEDUSA(9),HEDVSA(9),HEDWSA(9),HEDPDA(9),
     #HEDFAN(9),HEDIFL(9),HEDPAT(9),HEDRHO(9),HEDVIS(9),HEDCAL(9)
C
      COMMON
     #/CALIB/CPITCH(26),CDELTA(26),CVELCF(26),CPSTCF(26)
```

```
     #/MEASUR/RBETA(8,24),RPNMPS(8,24),RPCMPW(8,24),RPCMPA(8,24),
     #    NDATA(8),MAXJPT,RDNPRS(8),
     #    FANSPD(8),TFLOW(8),PATM(8),RZOFF(8)
     #/GEOM/X(8),R(24),XND(8),RND(24),DYPS(24),DYNP(24),
     #    SNS(24),NSTATN,XINCHS(8),RINCHS(24)
     #/CALC/VTOTAL(8,24),U(8,24),V(8,24),W(8,24),P(8,24),
     #    VTSTAR(8,24),USTAR(8,24),VSTAR(8,24),WSTAR(8,24),PSTAR(8,24),
     #    PICHCF(8,24),VELCF(8,24),DELTA(8,24),BETA(8,24),
     #    ANGMOM(8),UMEAN(8),MASS(8),MASFLO(8),UIN(8),
     #    PDIFF(8,24),PSTCF(8,24),AXMOM(8),AXMOMP(8),
     #    SPRIME(8),S(8),REDIN(8),PREF(8),RHO(8),VISCOS(8),
     #    USTAVG(8,24),VSTAVG(8,24),WSTAVG(8,24),PDFAVG(8,24)
     #/OUTPUT/STORE(8)
C
      REAL MASS,MASFLO
      LOGICAL IWRITE,DIAGNS
C
C---SET IWRITE=.TRUE. FOR WRITING SOLN. ON DISK STORAGE;
C   SET DIAGNS=.TRUE. TO ACTIVATE DIAGNOSTIC WRITE STATEMENTS .
C
      IWRITE=.TRUE.
      DIAGNS=.FALSE.
      IT=8
      JT=24
C
C---READ CHARACTER DATA FOR HEADINGS USED BY SUBROUTINES
C   WRITE AND PRINT (ALSO CALIBRATION HEADING)
C
      READ(5,205) HEDM,HEDUMN,HEDU,HEDV,HEDW,
     #    HEDVT,HEDUST,HEDVST,HEDWST,HEDPST,HEDDEL,HEDBET,
     #    HEDNMS,HEDCMW,HEDCMA,HEDMMF,HEDMIV,HEDMIP,HEDAM,
     #    HEDAX,HEDAXP,HEDSPR,HEDS,HEDP,HEDPDF,HEDRED,
     #    HEDFAN,HEDTFL,HEDPAT,HEDRHO,HEDVIS,
     #    HEDUSA,HEDVSA,HEDWSA,HEDPDA,HEDCAL
  205 FORMAT(9A4)
C
C---------INITIALIZE VARIABLES TO ZERO
C
      CALL INIT
C
C---------READ FIVE-HOLE PITOT CALIBRATION DATA
C
      NCAL=25
      DO 10 I=1,NCAL
        READ(5,210) CPITCH(I),CDELTA(I),CVELCF(I),CPSTCF(I)
   10 CONTINUE
  210 FORMAT(4F10.5)
      IF(DIAGNS) WRITE(6,400) (CPITCH(I),I=1,25)
      IF(DIAGNS) WRITE(6,400) (CDELTA(I),I=1,25)
      IF(DIAGNS) WRITE(6,400) (CVELCF(I),I=1,25)
      IF(DIAGNS) WRITE(6,400) (CPSTCF(I),I=1,25)
  400 FORMAT(///,1X,13(F8.4,1X),//,5X,12(F8.4))
C
C---READ USER HEADINGS, GEOMETRIC AND CONTROL PARAMETERS APPLYING
C   TO ENTIRE REDUCTION RUN
C
      READ(5,215) HEDID1,HEDID2
  215 FORMAT(18A4)
      READ(5,216) ALPHA,PHI,DSINCH,DLINCH
  216 FORMAT(4F10.5)
      READ(5,217) KRADTR,NSTATN,MAXJPT
  217 FORMAT(3I10)
C
C---READ EXPERIMENT PARAMETERS SPECIFIC TO EACH TRAVERSE, THEN
C   ACTUAL MEASUREMENT DATA IN TRAVERSE
C
```

```
      DO 30 I=1,NSTATN
        READ(5,230) XINCHS(I),NDATA(I),RDNPRS(I),PREF(I)
        READ(5,216) FANSPD(I),TFLOW(I),PATM(I),RZOFF(I)
        JPTS=NDATA(I)
        DO 20 J=1,JPTS
          READ(5,220) RINCHS(J),RBETA(I,J),RPNMPS(I,J),RPCMPW(I,J),
     #         RPCMPA(I,J)
   20   CONTINUE
   30 CONTINUE
C
C---------CONVERT X'S AND R'S FROM INCHES TO METERS
C
      RSMALL=DSINCH*0.0254/2.0
      RLARGE=DLINCH*0.0254/2.0
      DO 35 I=1,NSTATN
        X(I)=XINCHS(I)*0.0254
        JPTS=NDATA(I)
        DO 32 J=1,JPTS
          R(J)=RINCHS(J)*0.0254
   32   CONTINUE
   35 CONTINUE
  220 FORMAT(5F10.5)
  230 FORMAT(1F10.5,1I10,2F10.5)
      IF(DIAGNS) WRITE(6,470) (NDATA(I),I=1,NSTATN)
      IF(DIAGNS) WRITE(6,450) (X(I),I=1,NSTATN)
      IF(DIAGNS) WRITE(6,500) (R(J),J=1,JPTS)
      DO 37 I=1,NSTATN
        IF(DIAGNS) WRITE(6,500) (RBETA(I,J),J=1,JPTS)
        IF(DIAGNS) WRITE(6,500) (RPNMPS(I,J),J=1,JPTS)
        IF(DIAGNS) WRITE(6,500) (RPCMPW(I,J),J=1,JPTS)
        IF(DIAGNS) WRITE(6,500) (RPCMPA(I,J),J=1,JPTS)
   37 CONTINUE
  450 FORMAT(/,40X,1(F8.4,1X))
  470 FORMAT(///,40X,1(I8,1X))
  500 FORMAT(///,20X,10(F8.4))
C
CHAPTER  1  1  1  1  1  DATA REDUCTION  1  1  1  1  1  1
C
C---------CALC PICHCF AND INTERPOLATE FOR DELTA FROM
C---------        PITOT CALIBRATION CURVE
C
      IDID=0
      DO 50 I=1,NSTATN
        JPTS=NDATA(I)
        DO 40 J=1,JPTS
          IF((RPCMPW(I,J).EQ.0.0).AND.(RPNMPS(I,J).EQ.0.0)) GO TO 38
          PICHCF(I,J)=RPNMPS(I,J)/(RPCMPW(I,J)+1.E-6)
          IF((PICHCF(I,J).GT.2.544).OR.(PICHCF(I,J).LT.-3.769)) GO TO 38
          IF(IDID .EQ. 0) DELTA(I,J)=SPLINE(CPITCH,
     #      CDELTA,NCAL,PICHCF(I,J))
          IF(IDID .GT. 0) DELTA(I,J)=SP(CPITCH,CDELTA,
     #      NCAL,PICHCF(I,J))
          IDID=1
          GO TO 40
   38     CONTINUE
          DELTA(I,J)=0.0
          WRITE(6,850) I,J
  850     FORMAT(20X,'PICHCF IS OUT OF RANGE OF CALIBRATION AT I=
     #              ',I3,' AND J=',I3)
   40   CONTINUE
   50 CONTINUE
C
C---------INTERPOLATE FOR VELCF AND PSTCF FROM PITOT CALIBRATION DATA
C
      IDID=0
      DO 80 I=1,NSTATN
```

```
          JPTS=NDATA(I)
          DO 70 J=1,JPTS
            IF((RPCMPW(I,J).EQ.0.0).AND.(RPNMPS(I,J).EQ.0.0)) GO TO 65
            IF((ABS(DELTA(I,J))) .GT. 58.0) GO TO 65
            IF(IDID .EQ. 0) VELCF(I,J)=SPLINE(CDELTA,
     *        CVELCF,NCAL,DELTA(I,J))
            IF(IDID .GT. 0) VELCF(I,J)=SP(CDELTA,CVELCF,
     *        NCAL,DELTA(I,J))
            IF(IDID .EQ. 0) PSTCF(I,J)=SPLINE(CDELTA,
     *        CPSTCF,NCAL,DELTA(I,J))
            IF(IDID .GT. 0) PSTCF(I,J)=SP(CDELTA,CPSTCF,
     *        NCAL,DELTA(I,J))
            IDID=1
            GO TO 70
   65       CONTINUE
            VELCF(I,J)=0.0
            PSTCF(I,J)=0.0
            WRITE(6,890) I,J
  890       FORMAT(20X,'DELTA IS OUT OF RANGE OF CALIBRATION DATA
     *               AT I=',I3,' AND J=',I3)
   70     CONTINUE
   80 CONTINUE
C
        DO 85 I=1,NSTATN
          IF(DIAGNS) WRITE(6,500) (PICHCF(I,J),J=1,JPTS)
          IF(DIAGNS) WRITE(6,500) (DELTA(I,J),J=1,JPTS)
          IF(DIAGNS) WRITE(6,500) (VELCF(I,J),J=1,JPTS)
          IF(DIAGNS) WRITE(6,500) (PSTCF(I,J),J=1,JPTS)
   85 CONTINUE
C
C----------CALC MAGNITUDE OF TOTAL MEAN VELOCITY VECTOR,
C----------       U, V, & W COMPONENTS, AND STATIC PRESSURE
C
        PI=3.14159
        DO 100 I=1,NSTATN
          RHO(I)=PATM(I)*(133.33)/(286.94*(TFLOW(I)+273.15))
          JPTS=NDATA(I)
          DO 90 J=1,JPTS
            BETA(I,J)=360.+BZOFF(I)-RBETA(I,J)
            IF((RPCMPW(I,J).EQ.0.0).AND.(RPNMPS(I,J).EQ.0.0))BETA(I,J)=0.0
            VTOTAL(I,J)=SQRT(ABS(2.0/RHO(I)*VELCF(I,J)*RPCMPW(I,J)*133.33))
            U(I,J)=VTOTAL(I,J) * COS(DELTA(I,J)*PI/180.0) *
     *        COS(BETA(I,J)*PI/180.0)
            V(I,J)=VTOTAL(I,J) * SIN(DELTA(I,J)*PI/180.0)
            W(I,J)=VTOTAL(I,J) * COS(DELTA(I,J)*PI/180.0) *
     *        SIN(BETA(I,J)*PI/180.0)
            P(I,J)=(RPCMPA(I,J)-PSTCF(I,J)*RPCMPW(I,J))*133.33
   90     CONTINUE
  100 CONTINUE
        IF(DIAGNS) WRITE(6,500)(VTOTAL(I,J),J=1,JPTS)
        IF(DIAGNS) WRITE(6,500)(U(I,J),J=1,JPTS)
        IF(DIAGNS) WRITE(6,500)(V(I,J),J=1,JPTS)
        IF(DIAGNS) WRITE(6,500)(W(I,J),J=1,JPTS)
        IF(DIAGNS) WRITE(6,500)(P(I,J),J=1,JPTS)
C
CHAPTER  2  2  2  2  2  2  AUXILIARY CALCULATIONS  2  2  2  2  2
C
C------------NONDIMENSIONALIZE LENGTHS AND VELOCITIES
C
        DO 150 I=1,NSTATN
          XND(I)=X(I)/(2.0*RLARGE)
          JPTS=NDATA(I)
          UIN(I)=(SQRT(2.0/RHO(I)*RDNPFS(I)*133.33))*(6.312/5.938)**2
          MASFLO(I)=PI*RHO(I)*UIN(I)*RSMALL**2
          DO 140 J=1,JPTS
            VTSTAR(I,J)=VTOTAL(I,J)/UIN(I)
```

```
          USTAR(I,J)=U(I,J)/UIN(I)
          VSTAR(I,J)=V(I,J)/UIN(I)
          WSTAR(I,J)=W(I,J)/UIN(I)
          PSTAR(I,J)=P(I,J)/(RDNFRS(I)*133.33)
  140   CONTINUE
  150 CONTINUE
      IF(DIAGNS) WRITE(6,450) (UIN(I),I=1,NSTATN)
      IF(DIAGNS) WRITE(6,450) (MASFLO(I),I=1,NSTATN)
      DO 160 J=1,MAXJPT
        RND(J)=R(J)/(2.0*RLARGE)
        IF(KRADTR.EQ.0) RND(J)=RINCHS(J)
        IF(KRADTR.EQ.0) R(J)=RINCHS(J)
  160 CONTINUE
C
      IF(KRADTR.EQ.0) GO TO 135
C
C---FOR RADIAL PROFILES:  NUMERICAL INTEGRATION TO CALC. MASS
C   FLOW AND MOMENTUM FLUXES FOR SWIRL NUMBER
C
C   FOR PROFILES AT AND UPSTREAM OF EXPANSION CORNER, RSMALL
C   IS USED IN EXPRESSIONS FOR DYNP AND UMEAN; DOWNSTREAM OF
C   EXPANSION, RLARGE IS USED.
C
      DO 130 I=1,NSTATN
        JPTS=NDATA(I)
        JPTSM1=JPTS-1
        PREF(I)=P(I,JPTS)
        DYPS(1)=0.0
C
        IF(XINCHS(I).GT.0.0) GO TO 107
        DYNP(JPTS)=2.0*(RSMALL-R(JPTS))
        GO TO 108
  107   DYNP(JPTS)=2.0*(RLARGE-R(JPTS))
  108   CONTINUE
C
        DO 110 J=1,JPTSM1
          DYNP(J)=R(J+1)-R(J)
          DYPS(J+1)=DYNP(J)
  110   CONTINUE
        DO 115 J=1,JPTS
          SNS(J)=0.5*(DYNP(J)+DYPS(J))
          PDIFF(I,J)=P(I,J)-PREF(I)
  115   CONTINUE
C
C---INNER 3 (HUB) VALUES OF PDIFF ARE SET TO ZERO FOR SWIRLER
C   EXIT-PLANE PROFILES;  FOR DOWNSTREAM PROFILES, ACTUAL VALUES
C   ARE USED
C
        IF(XINCHS(I).GT.-1.28) GO TO 116
        PDIFF(I,1)=0.
        PDIFF(I,2)=0.
        PDIFF(I,3)=0.
  116   CONTINUE
C
        IF(DIAGNS) WRITE(6,500) (DYNP(J),J=1,JPTS)
        IF(DIAGNS) WRITE(6,500) (SNS(J),J=1,JPTS)
        AREA1=PI*SNS(1)**2
        ARSUM=AREA1
        FLOW=RHO(I)*U(I,1)*AREA1
        WMOM=W(I,1)*R(2)/4.*FLOW
        UMOM=U(I,1)*FLOW
        UMOMP=(RHO(I)*U(I,1)**2+PDIFF(I,1))*AREA1
        IF(DIAGNS) WRITE(6,2030) AREA1,ARSUM,FLOW,WMOM,UMOM,UMOMP
        DO 120 J=2,JPTS
          AREAJ=2.*PI*R(J)*SNS(J)
          ARSUM=ARSUM+AREAJ
```

ORIGINAL PAGE IS
OF POOR QUALITY

```
            FLOW=FLOW+RHO(I)*U(I,J)*AREAJ
            UMOM=UMOM+RHO(I)*U(I,J)**2*AREAJ
            UMOMP=UMOMP+(RHO(I)*U(I,J)**2+PDIFF(I,J))*AREAJ
            WMOM=WMOM+RHO(I)*U(I,J)*W(I,J)*R(J)*AREAJ
            IF(DIAGNS) WRITE(6,2040) AREAJ,ARSUM,FLOW,WMOM,UMOM,UMOMP
  120   CONTINUE
        MASS(I)=FLOW
C
        IF(XINCHS(I).GT.0.0) GO TO 122
        UMEAN(I)=MASS(I)/(RHO(I)*PI*RSMALL**2)
        GO TO 123
  122   UMEAN(I)=MASS(I)/(RHO(I)*PI*RLARGE**2)
  123   CONTINUE
C
        ANGMOM(I)=WMOM
        AXMOM(I)=UMOM
        AXMOMP(I)=UMOMP
        IF(DIAGNS) WRITE(6,2050) UMEAN(I),MASS(I),ANGMOM(I),AXMOM(I),
     #            AXMOMP(I)
C
 2030 FORMAT(//4X,'AREAJ',5X,'ARSUM',5X,'FLOW',6X,'WMOM',6X,
     #        'UMOM',6X,'UMOMP'//' ',6E10.3)
 2040 FORMAT(' ',6E10.3)
 2050 FORMAT(/14X,'UMEAN',5X,'MASS',6X,'ANGMOM',4X,'AXMOM',
     #        5X,'AXMOMP'//11X,5E10.3)
C
        SPRIME(I)=ANGMOM(I)/(AXMOM(I)*RSMALL)
        S(I)=ANGMOM(I)/(AXMOMP(I)*RSMALL)
  130 CONTINUE
      IF(DIAGNS) WRITE(6,450) (UMEAN(I),I=1,NSTATN)
      IF(DIAGNS) WRITE(6,450) (MASS(I),I=1,NSTAIN)
      IF(DIAGNS) WRITE(6,450) (ANGMOM(I),I=1,NSTATN)
      IF(DIAGNS) WRITE(6,450) (AXMOM(I),I=1,NSTATN)
      IF(DIAGNS) WRITE(6,450) (AXMOMP(I),I=1,NSTATN)
      IF(DIAGNS) WRITE(6,450) (SPRIME(I),I=1,NSTATN)
      IF(DIAGNS) WRITE(6,450) (S(I),I=1,NSTATN)
  135 CONTINUE
C
      IF(KRADTR.EQ.1) GO TO 180
C
C---FOR AZIMUTHAL TRAVERSES:  CALC. PDIFF=(P-PREF) USING SUPPLIED
C   VALUES OF PREF(I).
C
      DO 178 I=1,NSTATN
        JPTS=NDATA(I)
        DO 177 J=1,JPTS
          PDIFF(I,J)=P(I,J)-PREF(I)*133.33
  177   CONTINUE
  178 CONTINUE
C
C---CALC. AVERAGE VALUES FOR AZIMUTHAL TRAVERSES -- NREP IS NO. OF
C   POINTS IN REPEATING CYCLE ACROSS ONE BLADE; NAVE IS NO. OF
C   AVERAGES POSSIBLE CONTAINING NREP CONSECUTIVE POINTS.
C
      NREP=6
      DO 180 I=1,NSTATN
        NAVE=NDATA(I)-NREP+1
        DO 175 K=1,NAVE
          NAVEND=K+NREP-1
          USUM=0.
          VSUM=0.
          WSUM=0.
          PSUM=0.
          DO 174 J=K,NAVEND
            USUM=USUM+USTAR(I,J)
            VSUM=VSUM+VSTAR(I,J)
```

ORIGINAL PAGE IS
OF POOR QUALITY

```
              WSUM=WSUM+WSTAR(I,J)
              PSUM=PSUM+PDIFF(I,J)
  174       CONTINUE
            USTAVG(I,K)=USUM/NREF
            VSTAVG(I,K)=VSUM/NREF
            WSTAVG(I,K)=WSUM/NREF
            PDFAVG(I,K)=PSUM/NREF
  175     CONTINUE
  180 CONTINUE
C
C --CALCULATE VISCOSITY AND INLET REYNOLDS NUMBER (BOTH [illegible]
C
C---VISCOSITY FORMULA FROM LAN & ROSKAM, AIRPLANE AERODYNAMICS
C ' & PERFORMANCE, P.42.
C
      DO 162 I=1,NSTATN
        DENOM=TFLOW(I)+273.15+110.4
        VISCOS(I)=(1.458E-06)*(TFLOW(I)+273.15)**1.5/DENOM
        REDIN(I)=UIN(I)*2.*RSMALL*RHO(I)/VISCOS(I)
  162 CONTINUE
C
CHAPTER  3  3  3  3  3  OUTPUT  3  3  3  3  3  3  3
C
      IF(.NOT. IWRITE) GO TO 165
      WRITE(11) XINCHS
      WRITE(11) RINCHS
      WRITE(11) USTAR
      WRITE(11) VSTAR
      WRITE(11) WSTAR
      WRITE(11) BETA
      WRITE(11) DELTA
      WRITE(11) PDIFF
      WRITE(11) UIN
      WRITE(11) PREF
C
  165 CONTINUE
      WRITE(6,311)
      WRITE(6,312) HEDID1,HEDID2,HEDCAL
      WRITE(6,325) ALPHA
      WRITE(6,330) PHI
      WRITE(6,335) RSMALL
      WRITE(6,340) RLARGE
      CALL WRITE(1,1,NSTATN,1,II,JT,XINCHS,RINCHS,FANSPD,H[illegible]
      CALL WRITE(1,1,NSTATN,1,II,JT,XINCHS,RINCHS,TFLOW,HEDTFL)
      CALL WRITE(1,1,NSTATN,1,II,JT,XINCHS,RINCHS,PATM,HEDPAT)
      CALL WRITE(1,1,NSTATN,1,II,JT,XINCHS,RINCHS,RHO,HEDRHO)
      CALL WRITE(1,1,NSTATN,1,II,JT,XINCHS,RINCHS,VISCOS,HEDVIS)
      CALL WRITE(1,1,NSTATN,1,II,JT,XINCHS,RINCHS,REINFS,HEDRIF)
      CALL WRITE(1,1,NSTATN,1,II,JT,X,R,UIN,HEDUIN)
      CALL WRITE(1,1,NSTATN,1,II,JT,X,R,MASFLO,HEDMF)
      CALL WRITE(1,1,NSTATN,1,II,JT,X,R,REDIN,HEDRED)
C
      IF(KRADIR.EQ.0) GO TO 170
      CALL WRITE(1,1,NSTATN,1,II,JT,X,R,MASS,HEDM)
      CALL WRITE(1,1,NSTATN,1,II,JT,X,R,UMEAN,HEDUMN)
      CALL WRITE(1,1,NSTATN,1,IT,JT,X,R,ANGMOM,HEDAM)
      CALL WRITE(1,1,NSTATN,1,IT,JT,X,R,AXMOMP,HEDAXP)
      CALL WRITE(1,1,NSTATN,1,IT,JT,X,R,AXMOM,HEDAX)
      CALL WRITE(1,1,NSTATN,1,IT,JT,X,R,S,HEDS)
      CALL WRITE(1,1,NSTATN,1,IT,JT,X,R,SPRIME,HEDSPR)
C
  170 CONTINUE
      CALL PRINT(1,1,NSTATN,MAXJPT,IT,JT,X,R,U,HEDU)
      CALL PRINT(1,1,NSTATN,MAXJPT,IT,JT,X,R,V,HEDV)
      CALL PRINT(1,1,NSTATN,MAXJPT,IT,JT,X,R,W,HEDW)
      CALL PRINT(1,1,NSTATN,MAXJPT,IT,JT,X,R,P,HEDP)
```

```
      CALL PRINT(1,1,NSTATN,MAXJPT,IT,JT,X,R,DELTA,HEDDEL)
      CALL PRINT(1,1,NSTATN,MAXJPT,IT,JT,X,R,BETA,HEDBET)
      CALL PRINT(1,1,NSTATN,MAXJPT,IT,JT,X,R,VTOTAL,HEDVT)
      CALL PRINT(1,1,NSTATN,MAXJPT,IT,JT,XND,RND,USTAR,HEDUST)
      CALL PRINT(1,1,NSTATN,MAXJPT,IT,JT,XND,RND,VSTAR,HEDVST)
      CALL PRINT(1,1,NSTATN,MAXJPT,IT,JT,XND,RND,WSTAR,HEDWST)
      CALL PRINT(1,1,NSTATN,MAXJPT,IT,JT,XND,RND,PSTAR,HEDPST)
      CALL PRINT(1,1,NSTATN,MAXJPT,IT,JT,XND,RND,PDIFF,HEDPDF)
CC          CALL PRINT(1,1,NSTATN,MAXJPT,IT,JT,XND,RND,VTSTAR,HEDVT
C
      IF(KRADTR.EQ.1) GO TO 172
      CALL PRINT(1,1,NSTATN,MAXJPT,IT,JT,XINCHS,RINCHS,USTAVG,HEDUSA)
      CALL PRINT(1,1,NSTATN,MAXJPT,IT,JT,XINCHS,RINCHS,VSTAVG,HEDVSA)
      CALL PRINT(1,1,NSTATN,MAXJPT,IT,JT,XINCHS,RINCHS,WSTAVG,HEDWSA)
      CALL PRINT(1,1,NSTATN,MAXJPT,IT,JT,XINCHS,RINCHS,PDFAVG,HEDPDA)
C
  172 CONTINUE
      CALL PRINT(1,1,NSTATN,MAXJPT,IT,JT,XINCHS,RINCHS,RPNMPS,HEDNMS)
      CALL PRINT(1,1,NSTATN,MAXJPT,IT,JT,XINCHS,RINCHS,RPCMPW,HEDCMW)
      CALL PRINT(1,1,NSTATN,MAXJPT,IT,JT,XINCHS,RINCHS,RPCMPA,HEDCMA)
      STOP
C
C---------FORMAT STATEMENTS
C
  311 FORMAT(1H1,T37,'AXISYMMETRIC,ISOTHERMAL, GT COMBUSTOR FLOWFIELD ',
     $'MEASUREMENTS',//,T53,'USING A FIVE-HOLE PITOT PROBE')
  312 FORMAT(//T10,18A4/T10,18A4//T10,9A4)
  325 FORMAT(/T10,'EXPANSION ANGLE(DEG.) =',T50,1PE13.3)
  330 FORMAT(/T10,'SWIRL VANE ANGLE(DEG.) =',T50,1PE13.3)
  335 FORMAT (/T10,'INLET RADIUS(M) =',T50,1PE13.3)
  340 FORMAT(/T10,'COMBUSTOR RADIUS(M) =',T50,1PE13.3)
      END
C
      SUBROUTINE INIT
C*****************************************************************
C
      COMMON
     $/MEASUR/RBETA(8,24),RPNMPS(8,24),RPCMPW(8,24),RPCMPA(8,24),
     $    NDATA(8),MAXJPT,RDNPRS(8),
     $    FANSPD(8),TFLOW(8),PATM(8),BZOFF(8)
     $/GLOM/X(8),R(24),XND(8),RND(24),DYPS(24),DYNP(24),
     $    SNS(24),NSTATN,XINCHS(8),RINCHS(24)
     $/CALC/VTOTAL(8,24),U(8,24),V(8,24),W(8,24),P(8,24),
     $    VTSTAR(8,24),USTAR(8,24),VSTAR(8,24),WSTAR(8,24),PSTAR(8,24),
     $    PICHCF(8,24),VELCF(8,24),DELTA(8,24),BETA(8,24),
     $    ANGMOM(8),UMEAN(8),MASS(8),MASFLO(8),UIN(8),
     $    PDIFF(8,24),PSTCF(8,24),AXMOM(8),AXMOMP(8),
     $    SPRIME(8),S(8),REDIN(8),PREF(8),RHO(8),VISCOS(8),
     $    USTAVG(8,24),VSTAVG(8,24),WSTAVG(8,24),PDFAVG(8,24)
C
      REAL MASS,MASFLO
C
      DO 20 I=1,NSTATN
        MASFLO(I)=0.0
        MASS(I)=0.0
        ANGMOM(I)=0.0
        AXMOM(I)=0.0
        AXMOMP(I)=0.0
        SPRIME(I)=0.0
        S(I)=0.0
        UMEAN(I)=0.0
        UIN(I)=0.0
        DO 10 J=1,MAXJPT
          VTOTAL(I,J)=0.0
          U(I,J)=0.0
          V(I,J)=0.0
```

ORIGINAL PAGE IS
OF POOR QUALITY

```
            W(I,J)=0.0
            P(I,J)=0.0
            VTSTAR(I,J)=0.0
            USTAR(I,J)=0.0
            VSTAR(I,J)=0.0
            WSTAR(I,J)=0.0
            PSTAR(I,J)=0.0
            PDIFF(I,J)=0.0
            RBETA(I,J)=0.0
            BETA(I,J)=0.0
            RPNMPS(I,J)=0.0
            RPCMPW(I,J)=0.0
            RPCMPA(I,J)=0.0
            PICHCF(I,J)=0.0
            VELCF(I,J)=0.0
            PSTCF(I,J)=0.0
            DELTA(I,J)=0.0
            USTAVG(I,J)=0.0
            VSTAVG(I,J)=0.0
            WSTAVG(I,J)=0.0
            PDFAVG(I,J)=0.0
   10     CONTINUE
   20 CONTINUE
      RETURN
      END
C
      FUNCTION SPLINE(X, FX, N, X1)
C************************************************************************
C     CUBIC SPLINE CURVE FITTING IN 2 DIMENSIONAL DATA PLANE
C     INPUT VALUES :
C     X, FX      DATA ARRAYS, ONE DIMENSIONAL, X IN INCREASING ORDER
C     N          NUMBER OF DATA POINTS IN X, MAX 26
C     X1         POINT OF INTEREST, WHERE F(X1) IS TO BE FOUND
C
C     RETURN VALUE :
C     SPLINE OR SP = F(X1)
C     THIS ROUTINE ACTIVATES ROUTINE ABUILD, H, AND GAUSS.
C     FOR INTERPOLATION OF A LARGE NUMBER OF DATA POINTS, FUNCTION
C     SPLINE MAY BE CALLED ONLY ONCE , AND SUBSEQUENT CALLS MAY USE
C     ENTRY POINT SP.
C************************************************************************
      DIMENSION X(1), FX(1), A(26,27)
C
C---------CONSTRUCT SPLINE MATRIX
C
      N1=N+1
      DO 10  I=1, N
        DO 10  J=1, N1
   10     A(I,J)=0.
      M1=N-1
      DO 20  I=2, M1
   20   CALL ABUILD(X, FX, A, N, I)
      A(1,1)=H(X,2)
      A(1,2)=-H(X,1)-H(X,2)
      A(1,3)=H(X,1)
      M2=N-2
      A(N,M2)=H(X,M1)
      A(N,M1)=-H(X,M2)-H(X,M1)
      A(N,N)=H(X,M2)
C
C---------FIND SECOND DERIVATIVES
C
      CALL GAUSS(A, N, N1)
      ENTRY SP(X, FX, N, X1)
C
C---------FIND F(X1)
```

```
C
      DO 40  I=1, N1
        I1=I+1
        IF(X1 .EQ. X(I)) GO TO 50
        IF(X1 .LT. X(I) .AND. X1 .GT. X(I1)) GO TO 41
        IF(X1 .GT. X(I) .AND. X1 .LT. X(I1) ) GO TO 41
40    CONTINUE
      IF(X1 .EQ. X(N)) GO TO 60
      WRITE(6, 42) X1
42    FORMAT(' X1=', G14.7, ' OUT OF INTERPOLATION RANGE, RETURNED VALUE
     *=0')
      SP=0.
      SPLINE=0.
      STOP
C
41    CONTINUE
      I1=I+1
      HI=H(X,I)
      HX=X(I1)-X1
      HX2=X1-X(I)
      FX1=HX**3/HI-HI*HX
      FX1=FX1*A(I,N1)
      STO=HX2**3/HI - HI*HX2
      FX1=(FX1+STO*A(I1,N1) )/6.
      SPLINE=(FX(I)*HX+FX(I1)*HX2)/HI+FX1
      SP=SPLINE
      RETURN
C
50    CONTINUE
      SPLINE=FX(I)
      SP=SPLINE
      RETURN
C
60    CONTINUE
      SPLINE=FX(N)
      SP=SPLINE
      RETURN
      END
C
      FUNCTION H(X,I)
C***********************************************************************
C     CALCULATE DELTA X WHICH IS USUALLY CALLED H.
C***********************************************************************
      DIMENSION X(1)
      I1=I+1
      H=X(I1)-X(I)
      RETURN
      END
C
      SUBROUTINE ABUILD(X, F, A, N, I)
C***********************************************************************
C     CONSTRUCT  SPLINE MATRIX FOR FINDING 2ND DERIVATIVES
C***********************************************************************
      DIMENSION X(1), F(1), A(26,27)
      IM1=I-1
      I1=I+1
      N1=N+1
      STO=H(X,I)
      HIM1=H(X,IM1)
      A(I,IM1)=HIM1
      A(I,I)=2.*(HIM1+STO)
      A(I,I1)=STO
      A(I,N1)=( (F(I1)-F(I))/STO - (F(I)-F(IM1))/HIM1 )*6.
      RETURN
      END
C
```

```
      SUBROUTINE GAUSS(A, K, M)
C***********************************************************************
C     GAUSS-JORDAN ELIMINATION
C***********************************************************************
      DIMENSION A(26,27)
      M1=M-1
      K1=K-1
      DO 3  L=1, K1
        L1=L+1
        DO 3  I=L1, K
          CONST=A(I,L)/A(L,L)
          DO 3  J=L, M
    3       A(I,J)=A(I,J)-CONST*A(L,J)
      DO 6 I=1, K1
        I1=I+1
        DO 6  L=I1, M1
          CONST=A(I,L)/A(L,L)
          DO 6  J=I, M
6           A(I,J)=A(I,J)-CONST*A(L,J)
      DO 10  I=1, K
        A(I,M)=A(I,M)/A(I,I)
   10   A(I,I)=1.
      RETURN
      END
C
      SUBROUTINE PRINT(ISTART,JSTART,NI,NJ,IT,JT,X,Y,PHI,HEAD)
C***********************************************************************
C
      DIMENSION PHI(IT,JT),X(IT),Y(JT),HEAD(9)
      COMMON /OUTPUT/ STORE(8)
      ISKIP=1
      JSKIP=1
      WRITE(6,110)HEAD
      ISTA=ISTART-10
  100 CONTINUE
      ISTA=ISTA+10
      IEND=ISTA+9
      IF(NI.LT.IEND)IEND=NI
      WRITE(6,111)(I,I=ISTA,IEND,ISKIP)
      WRITE(6,114)(X(I),I=ISTA,IEND,ISKIP)
      WRITE(6,112)
      DO 101 JJ=JSTART,NJ,JSKIP
        J=JSTART+NJ-JJ
        DO 120 I=ISTA,IEND
          A=PHI(I,J)
          IF(ABS(A).LT.1.E-20) A=0.0
  120     STORE(I)=A
  101   WRITE(6,113)J,Y(J),(STORE(I),I=ISTA,IEND,ISKIP)
      IF(IEND.LT.NI)GO TO 100
      RETURN
  110 FORMAT(1H0,17(2H*-),7X,9A4,7X,17(2H-*))
  111 FORMAT(1H0,15H          I =    ,I2,9I11)
  112 FORMAT(8H0 J     Y)
  113 FORMAT(I3,0PF8.4,1X,10(1X,E10.3))
  114 FORMAT(13H          X = ,F8.4,9F11.4)
      END
C
      SUBROUTINE WRITE(ISTART,JSTART,NI,NJ,IT,JT,X,Y,PHI,HEAD)
C***********************************************************************
C
      COMMON /OUTPUT/ STORE(8)
      DIMENSION PHI(IT),X(IT),Y(JT),HEAD(9)
      ISKIP=1
      JSKIP=1
      WRITE(6,110)HEAD
      ISTA=ISTART-12
```

```
  100 CONTINUE
      ISTA=ISTA+12
      IEND=ISTA+11
      IF(NI.LT.IEND)IEND=NI
      WRITE(6,111)(I,I=ISTA,IEND,ISKIP)
      WRITE(6,114)(X(I),I=ISTA,IEND,ISKIP)
      DO 101 JJ=JSTART,NJ,JSKIP
        J=JSTART+NJ-JJ
        DO 120 I=ISTA,IEND
          A=PHI(I)
          IF(ABS(A).LT.1.E-20) A=0.0
  120     STORE(I)=A
  101   WRITE(6,113) (STORE(I),I=ISTA,IEND,ISKIP)
   .  IF(IEND.LT.NI)GO TO 100
      RETURN
  110 FORMAT(1H0,17(2H*-),7X,9A4,7X,17(2H-*))
  111 FORMAT(1H0,15H          I =     ,I2,9I11)
  113 FORMAT(/12X,1P10E11.3)
  114 FORMAT(13H          X =  ,F8.1,9F11.4)
      END
```

The following listing is of a dataset containing the input data for the reduction code. The two datasets are submitted together as a single batch job; they are merged by the computer before execution.

```
//GO.FT11F001 DD DSN='U12686A.NA70R21N.DATA',DISP=OLD
//GO.SYSIN DD *
   COMPUTED MASS FLOW RATE (KG/S)
 COMPUTED MEAN AXIAL VELOCITY (M/S)
         U VELOCITY (M/S)
         V VELOCITY (M/S)
         W VELOCITY (M/S)
   TOTAL VELOCITY MAGNITUDE (M/S)
      DIMENSIONLESS U VELOCITY
      DIMENSIONLESS V VELOCITY
      DIMENSIONLESS W VELOCITY
DIMENSIONLESS STATIC PRESS. P/RDNPRS
      PROBE PITCH ANGLE (DEG.)
       PROBE YAW ANGLE (DEG.)
    P(NORTH) - P(SOUTH)  (VOLTS)
    P(CENTER) - P(WEST)  (VOLTS)
    P(CENTER) - P(ATM.)  (VOLTS)
  MEAS. INLET MASS FLOW RATE (KG/S)
   MEAS. INLET AXIAL VELOCITY (M/S)
 MEAS. INLET DYNAMIC PRESS. (TORR)
AXIAL FLUX OF ANGULAR MOMENTUM (N-M)
AXIAL FLUX OF AXIAL MOM. (NEGL. PST)
AXIAL FLUX OF AXIAL MOM. (INCL. PST)
  SWIRL NO.  S-PRIME  (NEGL. PST)
     SWIRL NO.  S  (INCL. PST)
  STATIC PRESSURE, GAGE (N/SQ. M)
STAT. PRESS. DIFF., P-PREF (N/SQ.M)
       INLET REYNOLDS NUMBER
          FAN SPEED (RPM)
   REF. FLOW TEMP. (DEG CELSIUS)
    ATMOSPHERIC PRESSURE (TORR)
         DENSITY (KG/CU. M)
```

```
    ABS. (LAM.) VISCOSITY (KG/M-S)
    AVERAGES OF NONDIM. U-VELOCITY
    AVERAGES OF NONDIM. V-VELOCITY
    AVERAGES OF NONDIM. W-VELOCITY
AVERAGES OF STATIC PRESS. DIFFERENCE
CALIBRATION NO. 19 -- 10/10/82 (GFS)
 2.544     -58.0      1.661      -0.878
 2.233     -55.0      1.452      -0.602
 1.914     -50.0      1.289      -0.250
 1.608     -45.0      1.150       0.023
 1.365     -40.0      1.091       0.248
 1.155     -35.0      1.053       0.430
 0.966     -30.0      1.024       0.575
 0.801     -25.0      0.990       0.709
 0.663     -20.0      0.934       0.788
 0.537     -15.0      0.912       0.835
 0.412     -10.0      0.906       0.873
 0.270      -5.0      0.917       0.908
 0.110       0.0      0.912       0.915
-0.050       5.0      0.940       0.906
-0.209      10.0      0.946       0.880
-0.346      15.0      0.977       0.856
-0.476      20.0      1.017       0.823
-0.664      25.0      1.091       0.759
-0.896      30.0      1.196       0.664
-1.157      35.0      1.236       0.496
-1.487      40.0      1.300       0.278
-1.869      45.0      1.397       0.000
-2.319      50.0      1.541      -0.340
-3.063      55.0      1.892      -0.823
-3.769      58.0      2.300      -1.246
AZ. TRAV. AT R=2.1 FOR PHI=70, EXIT PLANE (NO BLOCK)
MEAS. 11/21/82 BY G. SANDER;  DATAFILE NAME 'NA70R21N'
90.0        70.0        5.938      11.75
              0          1          9
     -1.281            9       0.105       -.273
       2800.        38.0       741.4       0.0
-24.0       272.1      0.156      0.156       -.307
-18.0       270.6      0.143      0.170       -.307
-12.0       268.4      0.126      0.164       -.305
-6.0        268.9      0.116      0.136       -.310
0.0         268.4      0.120      0.112       -.313
6.0         268.0      0.131      0.099       -.316
12.0        266.4      0.144      0.118       -.323
18.0        267.2      0.150      0.134       -.326
24.0        269.3      0.141      0.140       -.326
//
```

Output generated by the reduction code using the example data given above appears on the following pages.

AXISYMMETRIC, ISOTHERMAL, GT COMBUSTOR FLOWFIELD MEASUREMENTS

USING A FIVE-HOLE PITOT PROBE

AZ. TRAV. AT R=2.1 FOR PHI=70, EXIT PLANE (NO BLOCK)
MEAS. 11/21/82 BY G. SANDER; DATAFILE NAME 'NA70R21N'

CALIBRATION NO. 19 -- 10/10/82 (GFS)

EXPANSION ANGLE(DEG.) = 9.000E+01

SWIRL VANE ANGLE(DEG.) = 7.000E+01

INLET RADIUS(M) = 7.541E-02

COMBUSTOR RADIUS(M) = 1.492E-01

FAN SPEED (RPM)

I = 1
X = -1.2810

2.800E+03

REP. FLOW TEMP. (DEG CELSIUS)

I = 1
X = -1.2810

3.800E+01

ATMOSPHERIC PRESSURE (TORR)

I = 1
X = -1.2810

7.414E+02

DENSITY (KG/CU. M)

I = 1
X = -1.2810

1.107E+00

ABS. (LAM.) VISCOSITY (KG/M-S)

I = 1
X = -1.2810

1.898E-05

MEAS. INLET DYNAMIC PRESS. (TORR)

I = 1
X = -1.2810

1.050E-01

MEAS. INLET AXIAL VELOCITY (M/S)

I = 1
X = -0.0325

5.682E+00

MEAS. INLET MASS FLOW RATE (KG/S)

I = 1
X = -0.0325

1.124E-01

INLET REYNOLDS NUMBER

I = 1
X = -0.0325

4.999E+04

U VELOCITY (M/S)

I = 1
X = -0.0325

J	Y	
9	24.0000	-0.618E-01
8	18.0000	-0.236E+00
7	12.0000	-0.279E+00
6	6.0000	-0.138E+00
5	0.0000	-0.125E+00
4	-6.0000	-0.987E-01
3	-12.0000	-0.159E+00
2	-18.0000	0.603E-01
1	-24.0000	0.196E+00

ORIGINAL PAGE IS
OF POOR QUALITY

V VELOCITY (M/S)

I = 1
X = -0.0325

J	Y	
9	24.0000	-0.306E+01
8	18.0000	-0.327E+01
7	12.0000	-0.330E+01
6	6.0000	-0.321E+01
5	0.0000	-0.288E+01
4	-6.0000	-0.258E+01
3	-12.0000	-0.253E+01
2	-18.0000	-0.285E+01
1	-24.0000	-0.320E+01

W VELOCITY (M/S)

I = 1
X = -0.0325

J	Y	
9	24.0000	0.506E+01
8	18.0000	0.482E+01
7	12.0000	0.443E+01
6	6.0000	0.396E+01
5	0.0000	0.446E+01
4	-6.0000	0.514E+01
3	-12.0000	0.571E+01
2	-18.0000	0.576E+01
1	-24.0000	0.534E+01

STATIC PRESSURE, GAGE (N/SQ. M)

I = 1
X = -0.0325

J	Y	
9	24.0000	-0.536E+02
8	18.0000	-0.516E+02
7	12.0000	-0.490E+02
6	6.0000	-0.459E+02
5	0.0000	-0.491E+02
4	-6.0000	-0.534E+02
3	-12.0000	-0.567E+02
2	-18.0000	-0.563E+02
1	-24.0000	-0.523E+02

PROBE PITCH ANGLE (DEG.)

I = 1
X = -0.0325

J	Y	
9	24.0000	-0.311E+02
8	18.0000	-0.341E+02
7	12.0000	-0.366E+02
6	6.0000	-0.390E+02
5	0.0000	-0.329E+02
4	-6.0000	-0.267E+02
3	-12.0000	-0.239E+02
2	-18.0000	-0.263E+02
1	-24.0000	-0.309E+02

PROBE YAW ANGLE (DEG.)

I = 1
X = -0.0325

J	Y	
9	24.0000	0.907E+02
8	18.0000	0.928E+02
7	12.0000	0.936E+02
6	6.0000	0.920E+02
5	0.0000	0.916E+02
4	-6.0000	0.911E+02
3	-12.0000	0.916E+02
2	-18.0000	0.894E+02
1	-24.0000	0.879E+02

TOTAL VELOCITY MAGNITUDE (M/S)

I = 1
X = -0.0325

J	Y	
9	24.0000	0.591E+01
8	18.0000	0.58[illegible]E+01
7	12.0000	0.553E+01
6	6.0000	0.510E+01
5	0.0000	0.531E+01
4	-6.0000	0.575E+01
3	-12.0000	0.624E+01
2	-18.0000	0.642E+01
1	-24.0000	0.623E+01

DIMENSIONLESS U VELOCITY

I = 1
X = -0.1090

J	Y	
9	24.0000	-0.109E-01
8	18.0000	-0.415E-01
7	12.0000	-0.490E-01
6	6.0000	-0.243E-01
5	0.0000	-0.219E-01
4	-6.0000	-0.174E-01
3	-12.0000	-0.280E-01
2	-18.0000	0.106E-01
1	-24.0000	0.345E-01

DIMENSIONLESS V VELOCITY

I = 1
X = -0.1090

J	Y	
9	24.0000	-0.538E+00
8	18.0000	-0.575E+00
7	12.0000	-0.580E+00
6	6.0000	-0.566E+00
5	0.0000	-0.507E+00
4	6.0000	-0.454E+00
3	12.0000	-0.445E+00
2	-18.0000	-0.501E+00
1	24.0000	-0.564E+00

DIMENSIONLESS W VELOCITY

I = 1
X = -0.1090

J	Y	
9	24.0000	0.890E+00
8	18.0000	0.849E+00
7	12.0000	0.779E+00
6	6.0000	0.697E+00
5	0.0000	0.785E+00
4	-6.0000	0.904E+00
3	-12.0000	0.100E+01
2	-18.0000	0.101E+01
1	-24.0000	0.940E+00

DIMENSIONLESS STATIC PRESS. P/RDNPRS

I = 1
X = -0.1090

J	Y	
9	24.0000	-0.383E+01
8	18.0000	-0.369E+01
7	12.0000	-0.350E+01
6	6.0000	-0.328E+01
5	0.0000	-0.351E+01
4	-6.0000	-0.382E+01
3	-12.0000	-0.405E+01
2	-18.0000	-0.402E+01
1	-24.0000	-0.374E+01

STAT. PRESS. DIFF., P-PREF (N/SQ.M)

I = 1
X = -0.1090

J	Y	
9	24.0000	-0.172E+02
8	18.0000	-0.152E+02
7	12.0000	-0.126E+02
6	6.0000	-0.951E+01
5	0.0000	-0.127E+02
4	-6.0000	-0.171E+02
3	-12.0000	-0.203E+02
2	-18.0000	-0.199E+02
1	-24.0000	-0.159E+02

AVERAGES OF NONDIM. U-VELOCITY

I = 1
X = -1.2810

J	Y	
9	24.0000	0.000E+00
8	18.0000	0.000E+00
7	12.0000	0.000E+00
6	6.0000	0.000E+00
5	0.0000	0.000E+00
4	-6.0000	-0.275E-01
3	-12.0000	-0.304E-01
2	-18.0000	-0.217E-01
1	-24.0000	-0.777E-02

AVERAGES OF NONDIM. V-VELOCITY

I = 1
X = -1.2810

J	Y	
9	24.0000	0.000E+00
8	18.0000	0.000E+00
7	12.0000	0.000E+00
6	6.0000	0.000E+00
5	0.0000	0.000E+00
4	-6.0000	-0.537E+00
3	-12.0000	-0.521E+00
2	-18.0000	-0.509E+00
1	-24.0000	-0.506E+00

AVERAGES OF NONDIM. W-VELOCITY

I = 1
X = -1.2810

J	Y	
9	24.0000	0.000E+00
8	18.0000	0.000E+00
7	12.0000	0.000E+00
6	6.0000	0.000E+00
5	0.0000	0.000E+00
4	-6.0000	0.817E+00
3	-12.0000	0.836E+00
2	-18.0000	0.864E+00
1	-24.0000	0.891E+00

AVERAGES OF STATIC PRESS. DIFFERENCE

I = 1
X = -1.2810

J	Y	
9	24.0000	0.000E+00
8	18.0000	0.000E+00
7	12.0000	0.000E+00
6	6.0000	0.000E+00
5	0.0000	0.000E+00
4	-6.0000	-0.141E+02
3	-12.0000	-0.146E+02
2	-18.0000	-0.153E+02
1	-24.0000	-0.159E+02

P(NORTH) P(SOUTH) (VOLTS)

I = 1
X = -1.2810

J	Y	
9	24.0000	0.141E+00
8	18.0000	0.150E+00
7	12.0000	0.144E+00
6	6.0000	0.131E+00
5	0.0000	0.120E+00
4	-6.0000	0.116E+00
3	-12.0000	0.126E+00
2	-18.0000	0.143E+00
1	-24.0000	0.156E+00

P(CENTER) - P(WEST) (VOLTS)

I = 1
X = -1.2810

J	Y	
9	24.0000	0.140E+00
8	18.0000	0.134E+00
7	12.0000	0.118E+00
6	6.0000	0.990E-01
5	0.0000	0.112E+00
4	-6.0000	0.136E+00
3	-12.0000	0.164E+00
2	-18.0000	0.170E+00
1	-24.0000	0.156E+00

P(CENTER) - P(ATM.) (VOLTS)

I = 1
X = -1.2810

J	Y	
9	24.0000	-0.326E+00
8	18.0000	-0.326E+00
7	12.0000	-0.323E+00
6	6.0000	-0.316E+00
5	0.0000	-0.313E+00
4	-6.0000	-0.310E+00
3	-12.0000	-0.305E+00
2	-18.0000	-0.307E+00
1	-24.0000	-0.307E+00